Phase structure of the on-shell parametrized 2 + 1 flavor Polyakov quark-meson model

Suraj Kumar Rai[1,2,*] and Vivek Kumar Tiwari[1,†]

[1]*Department of Physics, University of Allahabad, Prayagraj, India 211002*

[2]*Department of Physics, Acharya Narendra Deo Kisan P.G. College, Babhnan Gonda, India 271313*

(Received 22 June 2023; accepted 19 January 2024; published 26 February 2024)

Augmenting the improved chiral effective potential of the on-shell renormalized $2+1$ flavor quark-meson (RQM) model with the Polyakov-loop potential that accounts for the deconfinement transition, we get the quantum chromodynamics (QCD)-like framework of the renormalized Polyakov quark-meson (RPQM) model. When the divergent quark one-loop vacuum term is included in the effective potential of the quark-meson (QM) model, its tree-level parameters, or the parameters fixed by the use of meson curvature masses, become inconsistent as the curvature masses involve the self-energy evaluations at zero momentum. Using the modified minimal subtraction method, the consistent chiral effective potential for the RQM model has been calculated after relating the counterterms in the on-shell scheme to those in the $\overline{\text{MS}}$ scheme and finding the relations between the renormalized parameters of both the schemes where the physical (pole) masses of the π, K, η, and η' pseudoscalar mesons and the scalar σ meson, the pion and kaon decay constants, have been put into the relation of the running couplings and mass parameter. Using the RPQM model and the PQM model with different forms for the Polyakov-loop potentials in the presence or the absence of the quark backreaction, we have computed and compared the effect of the consistent quark one-loop correction and the quark backreaction on the scaled chiral order parameter, the QCD phase diagrams, and the different thermodynamic quantities. The results have been compared with the $2+1$ flavor lattice QCD data from the Wuppertal-Budapest Collaboration [J. High Energy Phys. 09 (2010) 73, Phys. Lett. B **730**, 99 (2014)] and the HotQCD Collaboration [Phys. Rev. D **90**, 094503 (2014)].

DOI: 10.1103/PhysRevD.109.034025

I. INTRODUCTION

The hadronic matter under the extreme conditions of high temperatures and/or densities gets dissolved into its quark and gluon constituents, and the quark gluon plasma (QGP) [1–5] is formed as predicted by the strong interaction theory quantum chromodynamics (QCD). The QCD phase diagram [1] and the general properties of QGP are subject matter of intensive investigation for the ultrarelativistic heavy ion collision experiments like the RHIC (BNL), LHC (CERN), and the upcoming CBM experiments at the FAIR facility (GSI-Darmstadt). The first-principle lattice QCD simulations [6–15] give us important information and insights for the QCD phase transition that occurs on the temperature axis, but when the baryon density is nonzero, these calculations get severely hampered as the QCD action becomes complex due to the fermion sign problem [8]. The QCD-like effective theory models [16–22] built upon the symmetries of the QCD give us the much needed framework in which the QCD phase structure and its thermodynamics can be explored in great details.

The QCD Lagrangian has the global $SU_{L+R}(3) \times SU_{L-R}(3)$ symmetry for the three massless quarks. The chiral (axial $A = L - R$) symmetry gets spontaneously broken in the low energy vacuum of the QCD, and one gets the nonstrange and the strange chiral condensates as the order parameters with eight massless pseudoscalar bosons as Goldstone modes. Since the small masses of the u and d quarks cause a small explicit breaking while a relatively large mass of the s quark generates a larger explicit breaking of the chiral symmetry, the three pions are light while the four kaons and one eta are heavier in nature. Due to the instanton effects, the $U_A(1)$ axial symmetry also gets explicitly broken to the $Z_A(N_f)$ at the quantum level [23]. The η' meson does not remain a massless Goldstone boson even when the quarks are massless as it acquires a mass of about 1 GeV due to the $U_A(1)$ axial anomaly. Coupling the nine scalar and nine pseudoscalar mesons of the three flavor linear sigma model [24] with the two light quarks u, d and the one heavier s quark, one gets the effective theory framework of the $2+1$ flavor quark-meson (QM) model [25].

*surajrai050@gmail.com

†vivekkrt@gmail.com

Several investigations of the QCD phase structure have already been done in the chiral models [24,26–39], two and three flavor QM model [25,40–43]. When the effect of the Dirac sea gets neglected in the standard mean field approximation (s-MFA), the QM model studies look inconsistent because in the chiral limit, the chiral phase transition at zero baryon density turns first order which is ruled out by the general theoretical arguments [44,45]. The inclusion of the quark one-loop vacuum fluctuation in the QM model [46] removes the above inconsistency. Investigations of the impact of fermionic vacuum fluctuations on the phase diagram of hot and dense QCD have a long history [46–53]. It was shown [49] that the phase diagram of the Polyakov-loop enhanced QM model is strongly affected by the fermionic vacuum contribution when the external magnetic field is present. The influence of the fermionic vacuum corrections (full two-loop results) have also been reported earlier in the context of finite temperature and density Yukawa theory [54–56]. Different QCD phase structure studies in the QM model with the quark one-loop vacuum term [52,53,57–68] showed that the fermionic vacuum fluctuations strongly influence the chiral phase transition, QCD phase diagram, and thermodynamics. In most of these studies, meson masses are defined by taking the double derivatives of the effective potential with respect to the different fields at its minimum. Such a definition known as the curvature mass is equivalent to defining the meson mass by using the self-energy that has been evaluated at zero momentum because the effective potential is the generator of the n-point functions of the theory at vanishing external momenta. The correct way of defining the meson mass in the hot gauge theories has a long history [69–73]. It has been emphasized [74,75] that the pole definition of the meson mass is the physical and gauge invariant one. The importance of determining the parameters in the Lagrangian in a consistent manner has been pointed out in Refs. [70–72] because if different definitions of masses are used or if tree-level relations are applied at the loop level, one cannot compare different model predictions quantitatively.

The tree-level relations between the physical quantities and the parameters of the Lagrangian are changed by the radiative corrections to the physical quantities. Hence, the use of the tree-level parameters in the effective potential become inconsistent. The running parameters in the $\overline{\mathrm{MS}}$ scheme have the renormalization scale Λ dependence while the on-shell parameters have their tree-level values. Following the correct renormalization prescription, when the counterterms calculated in the $\overline{\mathrm{MS}}$ scheme are put into the relations of the counterterms in the on-shell scheme, one finds the relations between the different renormalized parameters of the two schemes. The relations between the on-shell parameters (physical quantities) and the running $\overline{\mathrm{MS}}$ parameters are used as input when the effective potential is calculated using the modified minimal subtraction procedure [70]. Adhikari and collaborators [70,76–78] implemented the above on-shell parameter fixing in the two flavor QM model which uses the $O(4)$ sigma model with the σ and $\vec{\pi}$ mesons. In our recent works, we have calculated the consistent chiral effective potential for the on-shell renormalized two flavor [79] and $2+1$ flavor [80] quark-meson (RQM) model where the two and three flavor of quarks are, respectively, coupled to the eight and sixteen mesons of the corresponding $SU_L(2) \times SU_R(2)$ and $SU_L(3) \times SU_R(3)$ linear sigma model. We compared the results of the on-shell versus curvature mass parameter fixing schemes extensively when the quark one-loop vacuum correction is present in the two and three flavor quark-meson model and found that the effective potentials, order parameters, and phase diagrams which show nontrivial and significant σ mass dependent (i.e., $m_\sigma = 400$–700 MeV) differences are the same and coincident only for the $m_\sigma = 616$ MeV in the two flavor [79] and $m_\sigma = 648$–658 MeV for the three flavor case [80]. In contrast to the curvature mass parameter fixed quark-meson model with the vacuum term (QMVT) where the explicit symmetry breaking strengths h_x and h_y do not change, the strength h_x is reduced by a small amount while the strength h_y gets reduced by a relatively large amount in the $2+1$ flavor on-shell parameter fixed RQM model because the pion curvature mass $m_{\pi;c} = 135.95$ MeV is 2.05 MeV smaller than its physical mass $m_\pi = 138.0$ MeV, and the kaon curvature mass $m_{K;c} = 467.99$ MeV is 28.01 MeV smaller than its pole mass $m_K = 496.0$ MeV. Significant increase of the 't Hooft coupling c has also been found in the RQM model. On account of the above-mentioned reasons, the phase diagrams for the $2+1$ flavor case in the RQM model differ noticeably from those of the two flavor case, and the location of the critical end point (CEP) in the $2+1$ flavor RQM model shifts upward (toward the temperature axis) when compared to the two flavor case. In the curvature mass parameter fixed QMVT model, one gets an opposite trend of what one observes in the RQM model when the CEP for the $2+1$ flavor case shifts noticeably down in reference to the CEP of the two flavor case [80].

The physics of quark confinement in the hadrons is implemented by the Polyakov loop as the QCD confinement is mimicked in a statistical sense when the chiral models are coupled to a constant background $SU(N_c)$ gauge field A_μ^a [2,81–86]. When the free energy density from the gluons in the form of Polyakov-loop potential [87–89] is added to the QM model, it becomes the PQM model [90–94]. Very recently, we [95] augmented the consistent effective potential of the two flavor RQM model with the Polyakov-loop potential and studied the QCD thermodynamics and phase diagrams. Though the Polyakov-loop potential does not affect the vacuum parameters as it becomes active only at nonzero temperatures, combining the Polyakov-loop potential with the consistent and improved chiral effective potential of the $2+1$ flavor RQM Model, we get the more realistic QCD-like framework of the renormalized Polyakov

quark-meson model (RPQM) where we can investigate the interplay of the chiral symmetry breaking-restoration transition with the confinement-deconfinement transition. Since the Polyakov-loop potential is known to cause the upward shift of the CEP toward the temperature axis, it is important to quantitatively estimate how the novel feature of the upward shift of the CEP present in the $2+1$ flavor RQM model gets enhanced by the influence of the Polyakov-loop potential. In the earlier studies of the Polyakov-loop augmented curvature mass parameter fixed quark-meson model (PQMVT) with the vacuum term [58–61], the effect of fermionic vacuum correction looks overestimated as the CEP gets located in the far right corner of the phase diagram (closer to the chemical potential axis).

We have considered different parametrizations for the Polyakov-loop potentials along with the recent improvement in the form of the Polyakov-loop potential from a pure gauge potential to a unquenched glue potential in which the quark backreaction effects are included [96–99]. It is important to explore how the QCD phase structure computed in the present RPQM model framework gets modified by the unquenching of the Polyakov-loop potential because it leads to the linkage of the chiral and deconfinement phase transitions also at small temperatures and large chemical potentials [99]. The above feature is also noticed in the studies having the functional renormalization (FRG) improvement of the PQM model when the Yang-Mills Polyakov-loop potential is used [65,100]. In order to know the effect of the consistent quark one-loop vacuum correction, we have calculated the QCD phase diagrams and the QCD thermodynamics in the RPQM model and compared the results with that of the PQM model. Taking different forms of the Polyakov-loop potentials with and without quark backreaction, we have computed and compared how the phase structure gets influenced by the different implementations of the confinement-deconfinement physics in the RPQM model. The QCD thermodynamics has also been calculated in the curvature mass based parametrizon of the PQMVT model where quark backreaction is present, and the results obtained for different thermodynamic quantities have been compared with the corresponding calculations in the on-shell parametrized RRPQM model.

The organization of the paper is as follows. Section II presents a brief formulation of the $SU_L(3) \times SU_R(3)$ PQM model. The different forms of the Polyakov-loop potentials are described in Sec. II A, while Sec. II B gives the thermodynamic grand potential in the PQM model, and the parameters of the PQM model are determined in Sec. II C. Section III presents the effective potential of the on-shell renormalized Polyakov quark-meson model. Results and discussion are presented in Sec. IV. The comparisons of the thermodynamic quantities with the lattice QCD data have been discussed in Sec. IV A, and Sec. IV B illustrates and compares the phase diagrams and their CEP position in different model scenarios. Section V provides the summary and conclusion. Appendix A contains the important integrals and factors. The on-shell method of parameter fixing and derivation of the RQM model effective potential is presented in Appendix B.

II. MODEL FORMULATION

In the model [91–94], three flavor of quarks are coupled to the $SU_V(3) \times SU_A(3)$ symmetric mesonic fields together with the temporal component of the gauge field represented by the Polyakov-loop potential. The thermal expectation value of color trace of the Wilson loop in the temporal direction defines the Polyakov-loop field Φ as

$$\Phi(\vec{x}) = \frac{1}{N_c}\langle \mathrm{Tr}_c L(\vec{x})\rangle, \qquad \bar{\Phi}(\vec{x}) = \frac{1}{N_c}\langle \mathrm{Tr}_c L^{\dagger}(\vec{x})\rangle, \tag{1}$$

where $L(\vec{x})$ is a matrix in the fundamental representation of the $SU_c(3)$ color gauge group,

$$L(\vec{x}) = \mathcal{P}\exp\left[i\int_0^{\beta} d\tau A_0(\vec{x},\tau)\right]. \tag{2}$$

Here, $\mathcal{P}$ is path ordering, A_0 is the temporal component of vector field, and $\beta = T^{-1}$ [81]. As in the Refs. [87,88], the homogeneous Polyakov-loop fields $\Phi(\vec{x}) = \Phi =$ constant and $\bar{\Phi}(\vec{x}) = \bar{\Phi} =$ constant.

The Polyakov quark-meson (PQM) model Lagrangian is written in terms of the quarks, mesons, their couplings, and the Polyakov-loop potential $\mathcal{U}(\Phi, \bar{\Phi}, T)$ as

$$\mathcal{L}_{\mathcal{PQM}} = \mathcal{L}_{\mathcal{QM}} - \mathcal{U}(\Phi, \bar{\Phi}, T), \tag{3}$$

$$\mathcal{L}_{\mathcal{QM}} = \bar{\psi}[i\gamma^{\mu}D_{\mu} - gT_a(\sigma_a + i\gamma_5\pi_a)]\psi + \mathcal{L}(\mathcal{M}). \tag{4}$$

Here, ψ is a four-component Dirac spinor, a flavor triplet, and a color N_c-plet quark field,

$$\psi = \begin{pmatrix} u \\ d \\ s \end{pmatrix}. \tag{5}$$

The three flavor of quarks are coupled to the nine scalar $(\sigma_a, J^P = 0^+)$ and nine pseudoscalar $(\pi_a, J^P = 0^-)$ mesons by the flavor blind Yukawa coupling g. Quarks couple with the uniform temporal background gauge field as the following $D_{\mu} = \partial_{\mu} - iA_{\mu}$ and $A_{\mu} = \delta_{\mu 0}A_0$ (Polyakov gauge), where $A_{\mu} = g_s A^a_{\mu}\lambda^a/2$ with vector potential A^a_{μ} for color gauge field. g_s is the $SU_c(3)$ gauge coupling.

The Lagrangian for the meson fields is written as [25,26,94]

$$\mathcal{L}(\mathcal{M}) = \mathrm{Tr}(\partial_\mu \mathcal{M}^\dagger \partial^\mu \mathcal{M} - m^2(\mathcal{M}^\dagger \mathcal{M})) - \lambda_1[\mathrm{Tr}(\mathcal{M}^\dagger \mathcal{M})]^2 - \lambda_2 \mathrm{Tr}(\mathcal{M}^\dagger \mathcal{M})^2 + c[\det \mathcal{M} + \det \mathcal{M}^\dagger] + \mathrm{Tr}[H(\mathcal{M} + \mathcal{M}^\dagger)], \quad (6)$$

where the field $\mathcal{M}$ is a 3×3 complex matrix containing the nine scalars σ_a and the nine pseudoscalar π_a mesons,

$$\mathcal{M} = T_a \xi_a = T_a(\sigma_a + i\pi_a). \quad (7)$$

The T_a in the above are nine generators of $U(3)$ with $T_a = \frac{\lambda_a}{2}$ where $a = 0, 1, \ldots, 8$. The λ_a are standard Gell-Mann matrices with $\lambda_0 = \sqrt{\frac{2}{3}}\mathbb{I}_{3\times 3}$. The generators follow the $U(3)$ algebra $[T_a, T_b] = i f_{abc} T_c$ and $\{T_a, T_b\} = d_{abc} T_c$ where f_{abc} and d_{abc} are the standard antisymmetric and symmetric structure constants, respectively, with $f_{ab0} = 0$ and $d_{ab0} = \sqrt{\frac{2}{3}}\delta_{ab}$, and matrices are normalized as $\mathrm{Tr}(T_a T_b) = \frac{\delta_{ab}}{2}$. The $SU_L(3) \times SU_R(3)$ chiral symmetry is explicitly broken by the following term:

$$H = T_a h_a, \quad (8)$$

where H is a 3×3 matrix with nine parameters. Due to the spontaneous chiral symmetry breaking, the field ξ takes the nonzero vacuum expectation value, $\bar{\xi}$. Since $\bar{\xi}$ must have the quantum numbers of the vacuum, only three nonzero parameters h_0, h_3, and h_8 can cause the explicit breakdown of the chiral symmetry. Neglecting isospin symmetry breaking, we have taken h_0, $h_8 \neq 0$. One gets the $2+1$ flavor symmetry breaking scenario having the two nonzero condensates $\overline{\sigma_0}$ and $\overline{\sigma_8}$. In addition to the h_0 and h_8, the five other parameters of the model at tree level are the quartic coupling constants λ_1 and λ_2, squared mass parameter m^2, a Yukawa coupling g, and the coefficient of the 't Hooft determinant term c that models the $U_A(1)$ axial anomaly of the QCD vacuum.

A. Polyakov-loop potentials

Different forms of the Polyakov-loop effective potential $\mathcal{U}(\Phi, \bar{\Phi}, T)$, have been used in the literature to study the deconfinement phase transition. One constructs its simplest form by finding a potential which respects all the given symmetries and accounts for the spontaneously broken $Z(3)$ symmetry for the system in the deconfined phase [2,82,83]. The following polynomial form gives the minimal content of the Polyakov-loop potential:

$$\frac{\mathcal{U}_{\mathrm{Poly}}}{T^4} = -\frac{b_2(T)}{2}\Phi\bar{\Phi} - \frac{b_3}{6}(\Phi^3 + \bar{\Phi}^3) + \frac{b_4}{4}(\Phi\bar{\Phi})^2, \quad (9)$$

where the coefficients of Eq. (9) are given by

$$b_2(T) = a_0 + a_1\left(\frac{T_0}{T}\right) + a_2\left(\frac{T_0}{T}\right)^2 + a_3\left(\frac{T_0}{T}\right)^3, \quad (10)$$

where $a_0 = 6.75$, $a_1 = -1.95$, $a_2 = 2.625$, $a_3 = -7.44$, $b_3 = 0.75$, and $b_4 = 7.5$.

The Polyakov-loop potential in the above is improved by adding the contribution coming from the integration of the $SU(3)$ group volume in the generating functional for the Euclidean action. The Haar measure is used to perform this integration which takes the form of a Jacobian determinant. Its logarithm is added as an effective potential to the action in the generating functional. The positive coefficient of the logarithm term bounds the potential from below for large Φ and $\bar{\Phi}$, and the logarithmic form of the Polyakov-loop potential is written as [85,88]

$$\frac{\mathcal{U}_{\mathrm{Log}}}{T^4} = b(T)\ln[1 - 6\Phi\bar{\Phi} + 4(\Phi^3 + \bar{\Phi}^3) - 3(\Phi\bar{\Phi})^2] - \frac{1}{2}a(T)\Phi\bar{\Phi}. \quad (11)$$

The parameters of the polynomial and log form of the Polyakov-loop potential were determined [87,88] by fitting the lattice data for pressure and entropy density as well as energy density and the evolution of Polyakov loop $\langle\Phi\rangle$ on the lattice in pure gauge theory. The coefficients of Eq. (11) are the following [88]:

$$a(T) = a_0 + a_1\left(\frac{T_0}{T}\right) + a_2\left(\frac{T_0}{T}\right)^2, \quad (12)$$

$$b(T) = b_3\left(\frac{T_0}{T}\right)^3, \quad (13)$$

where $a_0 = 3.51$, $a_1 = -2.47$, $a_2 = 15.2$, $b_3 = -1.75$. One should note that the log potential has qualitative consistency with the leading order result of the strong-coupling expansion [15]. Also, because the potential diverges for $\Phi, \bar{\Phi} \to 1$, the Polyakov loop always remains smaller than 1 and approaches this value asymptotically as $T \to \infty$.

Accounting for the Polyakov-loop fluctuations, the new Polyakov-loop effective potential was constructed in Ref. [97] where the parameters get so adjusted that in addition to the other existing lattice data the longitudinal as well as the transverse susceptibilities are also reproduced. After the addition of the logarithmic term to the polynomial form of the Polyakov-loop potential, the new expression of the PolyLog Polyakov-loop potential in the above work has been found as the following:

TABLE I. Parameters of the PolyLog Polyakov-loop potential have been taken from Ref. [97].

PolyLog	$a_0^{(2)}$	$a_1^{(2)}$	$a_2^{(2)}$	$a_3^{(2)}$	$a_4^{(2)}$
	22.07	−75.7	45.03385	2.77173	3.56403
	$a_0^{(3)}$	$a_1^{(3)}$	$a_2^{(3)}$	$a_3^{(3)}$	$a_4^{(3)}$
	−25.39805	57.019	−44.7298	3.08718	6.72812
	$a_0^{(4)}$	$a_1^{(4)}$	$a_2^{(4)}$	$a_3^{(4)}$	$a_4^{(4)}$
	27.0885	−56.0859	71.2225	2.9715	6.61433
	b_0	b_1	b_2	b_3	
	−0.32665	5.8559	−82.9823	3.0	

$$\frac{\mathcal{U}_{\rm PolyLog}}{T^4} = b(T)\ln[1-6\Phi\bar{\Phi}+4(\Phi^3+\bar{\Phi}^3)-3(\Phi\bar{\Phi})^2] + a_2(T)\Phi\bar{\Phi}+a_3(T)(\Phi^3+\bar{\Phi}^3)+a_4(T)(\Phi\bar{\Phi})^2. \tag{14}$$

The coefficients of Eq. (14) PolyLog parametrization are defined as

$$a_i(T) = \frac{a_0^{(i)} + a_1^{(i)}\left(\frac{T_0}{T}\right) + a_2^{(i)}\left(\frac{T_0}{T}\right)^2}{1 + a_3^{(i)}\left(\frac{T_0}{T}\right) + a_4^{(i)}\left(\frac{T_0}{T}\right)^2} \tag{15}$$

$$b(T) = b_0\left(\frac{T_0}{T}\right)^{b_1}[1-e^{b_2(\frac{T_0}{T})^{b_3}}]. \tag{16}$$

The parameters are summarized in Table I.

For the pure gauge Yang-Mills theory, the deconfinement phase transition is first order, and $T_c^{\rm YM} = T_0 = 270$ MeV. When the dynamical quarks are present, the first order transition becomes a crossover. The parameter T_0 depends on the number of quark flavors and chemical potential in the full dynamical QCD [67,90,96,99,100] as it is linked to the mass-scale $\Lambda_{\rm QCD}$ which gets modified by the effect of the fermionic matter fields. The number of flavors and the chemical potential dependence of $T_0 \to T_0(N_f,\mu)$ are written as

$$T_0(N_f,\mu) = \hat{T}e^{-1/(\alpha_0 b(N_f,\mu))}, \tag{17}$$

with

$$b(N_f,\mu) = \frac{1}{6\pi}(11N_c - 2N_f) - b_\mu\frac{\mu^2}{(\hat{\gamma}\,\hat{T})^2}, \tag{18}$$

where the parameter $\hat{T}$ is fixed at the scale τ, $\hat{T} = T_\tau = 1.77$ GeV, and $\alpha_0 = \alpha(\Lambda)$ at a UV scale Λ. The $T_0(N_f = 0) = 270$ MeV gives $\alpha_0 = 0.304$ and $b_\mu \simeq \frac{16}{\pi}N_f$. The parameter $\hat{\gamma}$ governs the curvature of $T_0(\mu)$ with the systematic error estimation range $0.7 \lesssim \hat{\gamma} \lesssim 1$ [90,100]. Massive flavors lead to suppression factors of the order $T_0^2/(T_0^2+m^2)$ in the β function. For $2+1$ flavors and a current strange quark mass $m_s \sim 150$ MeV, one obtains $T_0(2+1) = 187$ MeV [90,100].

When the backreaction of the quarks is accounted for, in the full QCD with dynamical quarks, the Polyakov-loop potential gets replaced by the QCD glue potential. Reference [96] applied the FRG equations to the QCD and compared the pure gauge potential $\mathcal{U}_{\rm YM}$ to the "glue" potential $\mathcal{U}_{\rm glue}$ where quark polarization was included in the gluon propagator, and they found significant differences between the two potentials. However, it was observed that the two potentials are of the same shape, and they can be mapped into each other by relating the temperatures of the two systems, $T_{\rm YM}$ and $T_{\rm glue}$. Denoting the previous equations of the Polyakov-loop potential by $\mathcal{U}_{\rm YM}$, the improved Polyakov-loop potential $\mathcal{U}_{\rm glue}$ can be constructed as [96]

$$\frac{\mathcal{U}_{\rm glue}}{T_{\rm glue}^4}(\Phi,\bar{\Phi},T_{\rm glue}) = \frac{\mathcal{U}_{\rm YM}}{T_{\rm YM}^4}(\Phi,\bar{\Phi},T_{\rm YM}), \tag{19}$$

where the temperature $T_{\rm glue}$ is related to $T_{\rm YM}$ as

$$\frac{T_{\rm YM}-T_{\rm c}^{\rm YM}}{T_{\rm c}^{\rm YM}} = 0.57\frac{T_{\rm glue}-T_{\rm c}^{\rm glue}}{T_{\rm c}^{\rm glue}}. \tag{20}$$

The transition temperature for the unquenched case is the $T_{\rm c}^{\rm glue}$. The coefficient 0.57 comes from the comparison of the two effective potentials. $T_{\rm c}^{\rm glue}$ lies within a range $T_{\rm c}^{\rm glue} \in [180, 270]$. In practice, one uses the replacement $T \to T_{\rm c}^{\rm YM}(1+0.57(\frac{T}{T_{\rm c}^{\rm glue}}-1))$ in the right-hand side of the Polyakov-loop potentials where T_0 means $T_{\rm c}^{\rm YM}$ and $(T \sim T_{\rm YM})$ on the left side of the arrow while $(T \sim T_{\rm glue})$ on the right side. In our calculations, we have taken $T_{\rm c}^{\rm glue}$ and T_0 both fixed at 187 MeV for the $2+1$ quark flavor as in Refs. [90,96].

B. Grand potential in the mean field approach

We have the spatially uniform system that is in the thermal equilibrium at temperature T and quark chemical potential $\mu_f (f = u,d,s)$. The partition function is calculated by performing the path integral over the quark/antiquark and meson fields [25,94],

$$\mathcal{Z} = {\rm Tr}\,\exp\left[-\beta\left(\hat{\mathcal{H}} - \sum_{f=u,d,s}\mu_f\hat{\mathcal{N}}_f\right)\right] = \int\prod_a \mathcal{D}\sigma_a\mathcal{D}\pi_a\int\mathcal{D}\psi\mathcal{D}\bar{\psi}\exp\left[-\int_0^\beta d\tau\int_V d^3x \times\left(\mathcal{L}^{\mathcal{E}}_{\mathcal{QM}} + \sum_{f=u,d,s}\mu_f\bar{\psi}_f\gamma^0\psi_f\right)\right]. \tag{21}$$

Here, $\beta = \frac{1}{T}$, and the volume of the system in the three dimension is V. There will be three chemical potentials for the three flavor of quarks, and the $SU_V(2)$ symmetry is assumed to be preserved as the small difference in the mass of u and d quark gets neglected. Hence, the quark chemical potential for the u and d quarks is equal $\mu_u = \mu_d$, and the strange quark chemical potential is μ_s.

In the standard mean-field approximation [25,40,94], the partition function is calculated by replacing the meson fields with their vacuum expectation values $\langle M \rangle = T_0\overline{\sigma_0} + T_8\overline{\sigma_8}$ and neglecting the thermal as well as quantum fluctuations of the meson fields while retaining the quarks and antiquarks as quantum fields. Now, following the standard procedure as given in Refs. [91–94,101], one can obtain the expression of grand potential as the sum of pure gauge field contribution $\mathcal{U}(\Phi, \bar{\Phi}, T)$, meson contribution, and quark/antiquark contribution evaluated in the presence of a Polyakov loop,

$$\Omega_{\rm MF}(T,\mu) = U(\overline{\sigma_0}, \overline{\sigma_8}) + \Omega_{q\bar{q}}(T,\mu;\overline{\sigma_0}, \overline{\sigma_8}, \Phi, \bar{\Phi}) + \mathcal{U}(T, \Phi, \bar{\Phi}). \tag{22}$$

The $2+1$ flavor case can be explored after implementing the basis transformation of the condensates and the external fields from the original singlet octet (0, 8) basis to the nonstrange strange basis ($\bar{\sigma}_x$, $\bar{\sigma}_y$),

$$\bar{\sigma}_x = \sqrt{\frac{2}{3}}\bar{\sigma}_0 + \frac{1}{\sqrt{3}}\bar{\sigma}_8, \tag{23}$$

$$\bar{\sigma}_y = \frac{1}{\sqrt{3}}\bar{\sigma}_0 - \sqrt{\frac{2}{3}}\bar{\sigma}_8. \tag{24}$$

The grand potential is written in $\bar{\sigma}_x$, $\bar{\sigma}_y$ basis as

$$\Omega_{\rm MF}(T,\mu) = U(\bar{\sigma}_x, \bar{\sigma}_y) + \mathcal{U}(T, \Phi, \bar{\Phi}) + \Omega_{q\bar{q}}(T,\mu;\bar{\sigma}_x, \bar{\sigma}_y, \Phi, \bar{\Phi}). \tag{25}$$

The external fields (h_x, h_y) can be written in terms of the (h_0, h_8) by similar expressions. Since the nonstrange and strange quark/antiquark decouple, the quark masses are written as

$$m_u = g\frac{\bar{\sigma}_x}{2}, \qquad m_s = g\frac{\bar{\sigma}_y}{\sqrt{2}}. \tag{26}$$

One writes the tree-level effective potential in the nonstrange-strange basis as the following:

$$U(\bar{\sigma}_x, \bar{\sigma}_y) = \frac{m^2}{2}(\bar{\sigma}_x^2 + \bar{\sigma}_y^2) - h_x\bar{\sigma}_x - h_y\bar{\sigma}_y - \frac{c}{2\sqrt{2}}\bar{\sigma}_x^2\bar{\sigma}_y + \frac{\lambda_1}{2}\bar{\sigma}_x^2\bar{\sigma}_y^2 + \frac{1}{8}(2\lambda_1 + \lambda_2)\bar{\sigma}_x^4 + \frac{1}{8}(2\lambda_1 + 2\lambda_2)\bar{\sigma}_y^4. \tag{27}$$

Applying the stationarity conditions $\frac{\partial U(\bar{\sigma}_x,\bar{\sigma}_y)}{\partial \bar{\sigma}_x} = 0 = \frac{\partial U(\bar{\sigma}_x,\bar{\sigma}_y)}{\partial \bar{\sigma}_y}$ to the effective potential (27), one gets

$$h_x = \bar{\sigma}_x m_\pi^2, \tag{28}$$

$$h_y = \left\{\frac{\sqrt{2}}{2}(m_K^2 - m_\pi^2)\bar{\sigma}_x + m_K^2\bar{\sigma}_y\right\}. \tag{29}$$

The tree-level curvature masses of the pions, kaons, and other mesons in the QM model are given by the mass matrix $(m_{\alpha,ab})^2$ evaluated in Refs. [24,25]. Here, $\alpha =$ s, p; "s" stands for the scalar, "p" stands for the pseudoscalar mesons, and $a, b = 0, 1, 2, \ldots, 8$. In the scalar sector, the a_0 meson mass is given by the 11 elements (degenerate with the 22 and 33 elements), and the κ meson mass is given by the 44 elements (degenerate with the 55, 66, and 77 elements). The σ and f_0 meson masses are found by diagonalizing the (00)-(88) sector of the scalar mass matrix. In an exactly analogous manner for the pseudoscalar sector, $m^2_{\rm p,11} = m^2_{\rm p,22} = m^2_{\rm p,33} \equiv m_\pi^2$ and $m^2_{\rm p,44} = m^2_{\rm p,55} = m^2_{\rm p,66} = m^2_{\rm p,77} \equiv m_K^2$. Diagonalization of the pseudoscalar (00)-(88) sector of the mass matrix gives us the masses of the physical η and η' mesons. Table II contains masses of all the mesons.

The quark/antiquark contribution is given by

$$\Omega_{q\bar{q}}(T,\mu;\bar{\sigma}_x,\bar{\sigma}_y,\Phi,\bar{\Phi}) = \Omega^{\rm vac}_{q\bar{q}} + \Omega^{T,\mu}_{q\bar{q}}, \tag{30}$$

$$\Omega^{\rm vac}_{q\bar{q}} = -2N_c\sum_f \int \frac{d^3p}{(2\pi)^3} E_f\theta(\Lambda_c^2 - \vec{p}^2), \tag{31}$$

$$\Omega^{T,\mu}_{q\bar{q}} = -2\sum_f \int \frac{d^3p}{(2\pi)^3} T[\ln g_f^+ + \ln g_f^-]. \tag{32}$$

The first term of Eq. (30) is the contribution of the fermion vacuum fluctuation, where Λ_c is the ultraviolet cutoff. In the presence of the Polyakov-loop potential, g_f^+ and g_f^- are specified by the trace in the color space,

$$g_f^+ = [1 + 3\Phi e^{-E_f^+/T} + 3\bar{\Phi}e^{-2E_f^+/T} + e^{-3E_f^+/T}], \tag{33}$$

$$g_f^- = [1 + 3\bar{\Phi} e^{-E_f^-/T} + 3\Phi e^{-2E_f^-/T} + e^{-3E_f^-/T}]. \tag{34}$$

$E_f^\pm = E_f \mp \mu_f$ and $E_f = \sqrt{p^2 + {m_f}^2}$ is the flavor dependent single particle energy of the quark/antiquark, $m_u = m_d = \frac{g\bar{\sigma}_x}{2}$ is the mass of the light quarks u, d, and strange quark mass is $m_s = \frac{g\bar{\sigma}_y}{\sqrt{2}}$. For the present work, it is assumed that $\mu_u = \mu_d = \mu_s = \mu$.

The quark one-loop vacuum term of Eq. (30) is neglected in the standard mean-field approximation (s-MFA), and the grand potential of the PQM model is written as

TABLE II. Meson masses calculated from the second derivative of the grand potential at its minimum as given in Refs. [25,31].

Scalar meson masses		Pseudoscalar meson masses	
$(m_{a_0})^2$	$m^2+\lambda_1(\bar{\sigma}_x^2+\bar{\sigma}_y^2)+\frac{3\lambda_2}{2}\bar{\sigma}_x^2+\frac{\sqrt{2}c}{2}\bar{\sigma}_y$	$(m_\pi)^2$	$m^2+\lambda_1(\bar{\sigma}_x^2+\bar{\sigma}_y^2)+\frac{\lambda_2}{2}\bar{\sigma}_x^2-\frac{\sqrt{2}c}{2}\bar{\sigma}_y$
$(m_\kappa)^2$	$m^2+\lambda_1(\bar{\sigma}_x^2+\bar{\sigma}_y^2)+\frac{\lambda_2}{2}(\bar{\sigma}_x^2+\sqrt{2}\bar{\sigma}_x\bar{\sigma}_y+2\bar{\sigma}_y^2)+\frac{c}{2}\bar{\sigma}_x$	$(m_K)^2$	$m^2+\lambda_1(\bar{\sigma}_x^2+\bar{\sigma}_y^2)+\frac{\lambda_2}{2}(\bar{\sigma}_x^2-\sqrt{2}\bar{\sigma}_x\bar{\sigma}_y+2\bar{\sigma}_y^2)-\frac{c}{2}\bar{\sigma}_x$
$(m_{s,00})^2$	$m^2+\frac{\lambda_1}{3}(7\bar{\sigma}_x^2+4\sqrt{2}\bar{\sigma}_x\bar{\sigma}_y+5\bar{\sigma}_y^2)+\lambda_2(\bar{\sigma}_x^2+\bar{\sigma}_y^2)-\frac{\sqrt{2}c}{3}(\sqrt{2}\bar{\sigma}_x+\bar{\sigma}_y)$	$(m_{p,00})^2$	$m^2+\lambda_1(\bar{\sigma}_x^2+\bar{\sigma}_y^2)+\frac{\lambda_2}{3}(\bar{\sigma}_x^2+\bar{\sigma}_y^2)+\frac{c}{3}(2\bar{\sigma}_x+\sqrt{2}\bar{\sigma}_y)$
$(m_{s,88})^2$	$m^2+\frac{\lambda_1}{3}(5\bar{\sigma}_x^2-4\sqrt{2}\bar{\sigma}_x\bar{\sigma}_y+7\bar{\sigma}_y^2)+\lambda_2(\frac{\bar{\sigma}_x^2}{2}+2\bar{\sigma}_y^2)+\frac{\sqrt{2}c}{3}(\sqrt{2}\bar{\sigma}_x-\frac{\bar{\sigma}_y}{2})$	$(m_{p,88})^2$	$m^2+\lambda_1(\bar{\sigma}_x^2+\bar{\sigma}_y^2)+\frac{\lambda_2}{6}(\bar{\sigma}_x^2+4\bar{\sigma}_y^2)-\frac{c}{6}(4\bar{\sigma}_x-\sqrt{2}\bar{\sigma}_y)$
$(m_{s,08})^2$	$\frac{2\lambda_1}{3}(\sqrt{2}\bar{\sigma}_x^2-\bar{\sigma}_x\bar{\sigma}_y-\sqrt{2}\bar{\sigma}_y^2)+\sqrt{2}\lambda_2(\frac{\bar{\sigma}_x^2}{2}-\bar{\sigma}_y^2)+\frac{c}{3\sqrt{2}}(\bar{\sigma}_x-\sqrt{2}\bar{\sigma}_y)$	$(m_{p,08})^2$	$\frac{\sqrt{2}\lambda_2}{6}(\bar{\sigma}_x^2-2\bar{\sigma}_y^2)-\frac{c}{6}(\sqrt{2}\bar{\sigma}_x-2\bar{\sigma}_y)$
$(m_{s,xx})^2$	$m^2+3(\lambda_1+\frac{\lambda_2}{2})\bar{\sigma}_x^2+\lambda_1\bar{\sigma}_y^2-\frac{c}{\sqrt{2}}\bar{\sigma}_y$	$(m_{p,xx})^2$	$m^2+(\lambda_1+\frac{\lambda_2}{2})\bar{\sigma}_x^2+\lambda_1\bar{\sigma}_y^2+\frac{c}{\sqrt{2}}\bar{\sigma}_y$
$(m_{s,yy})^2$	$m^2+\lambda_1\bar{\sigma}_x^2+3(\lambda_1+\lambda_2)\bar{\sigma}_y^2$	$(m_{p,yy})^2$	$m^2+\lambda_1\bar{\sigma}_x^2+(\lambda_1+\lambda_2)\bar{\sigma}_y^2$
$(m_{s,xy})^2$	$2\lambda_1\bar{\sigma}_x\bar{\sigma}_y-\frac{c}{\sqrt{2}}\bar{\sigma}_x$	$(m_{p,xy})^2$	$\frac{c}{\sqrt{2}}\bar{\sigma}_x$
m_σ^2	$\frac{1}{2}(m_{s,00}^2+m_{s,88}^2)-\frac{1}{2}\sqrt{(m_{s,00}^2-m_{s,88}^2)^2+4m_{s,00}^4}$	m_η^2	$\frac{1}{2}(m_{p,00}^2+m_{p,88}^2)-\frac{1}{2}\sqrt{(m_{p,00}^2-m_{p,88}^2)^2+4m_{p,00}^4}$
$m_{f_0}^2$	$\frac{1}{2}(m_{s,00}^2+m_{s,88}^2)+\frac{1}{2}\sqrt{(m_{s,00}^2-m_{s,88}^2)^2+4m_{s,00}^4}$	$m_{\eta'}^2$	$\frac{1}{2}(m_{p,00}^2+m_{p,88}^2)+\frac{1}{2}\sqrt{(m_{p,00}^2-m_{p,88}^2)^2+4m_{p,00}^4}$

$$\Omega_{\rm PQM}(T,\mu,\bar{\sigma}_x,\bar{\sigma}_y,\Phi,\bar{\Phi})=U(\bar{\sigma}_x,\bar{\sigma}_y)+\mathcal{U}(T,\Phi,\bar{\Phi})+\Omega_{q\bar{q}}(T,\mu;\bar{\sigma}_x,\bar{\sigma}_y,\Phi,\bar{\Phi}). \quad (35)$$

The grand minima of the thermodynamic potential given by Eq. (35) gives $\bar{\sigma}_x$, $\bar{\sigma}_y$, Φ, and $\bar{\Phi}$ by

$$\frac{\partial\Omega_{\rm PQM}}{\partial\bar{\sigma}_x}=\frac{\partial\Omega_{\rm PQM}}{\partial\bar{\sigma}_y}=\frac{\partial\Omega_{\rm PQM}}{\partial\Phi}=\frac{\partial\Omega_{\rm PQM}}{\partial\bar{\Phi}}=0. \quad (36)$$

C. Parameters of the QM model

The experimental values of the pion and kaon mass, the average squared mass of the pseudoscalars η and η' mesons $(m_\eta^2+m_{\eta'}^2)$, the scalar σ meson mass m_σ, and the pion and kaon decay constants f_π and f_K are used as the input [24,25] for determining the six model parameters m^2, λ_1, λ_2, c, h_x, and h_y.

The values of the condensates in the vacuum are $\bar{\sigma}_x=f_\pi$ and $\bar{\sigma}_y=(2f_K-f_\pi)/\sqrt{2}$ according to the partially conserved axial-vector current relation (PCAC). The above values of condensates at $T=0,\mu=0$ give the minimum of the vacuum effective potential in Eq. (36). The parameters λ_2 and c in the vacuum are given by

$$\lambda_2=\frac{2}{(\bar{\sigma}_x^2+4\bar{\sigma}_y^2)(\sqrt{2}\bar{\sigma}_y-\bar{\sigma}_x)}[(3\sqrt{2}\bar{\sigma}_y)m_K^2-(\sqrt{2}\bar{\sigma}_y+2\bar{\sigma}_x)m_\pi^2-(\sqrt{2}\bar{\sigma}_y-\bar{\sigma}_x)(m_\eta^2+m_{\eta'}^2)], \quad (37)$$

$$c=\frac{2(m_K^2-m_\pi^2)}{(\sqrt{2}\bar{\sigma}_y-\bar{\sigma}_x)}-\sqrt{2}\bar{\sigma}_y\lambda_2. \quad (38)$$

The mass parameter m^2 gets canceled in the difference of the σ and π mass squares $(m_\sigma^2-m_\pi^2)$. The difference $(m_\sigma^2-m_\pi^2)$ depends on the parameters λ_1, λ_2, and c. When the λ_2 and c calculated from the above equations are put into the expression of $(m_\sigma^2-m_\pi^2)$ with $\bar{\sigma}_x=f_\pi$ and $\bar{\sigma}_y=(2f_K-f_\pi)/\sqrt{2}$, one gets the vacuum value of the parameter λ_1. The mass parameter m^2 can be obtained from the expression of the m_π^2 as the following:

$$m^2=m_\pi^2-\lambda_1(\bar{\sigma}_x^2+\bar{\sigma}_y^2)-\frac{\lambda_2}{2}\bar{\sigma}_x^2+\frac{c}{\sqrt{2}}\bar{\sigma}_y. \quad (39)$$

Putting the vacuum values of m_π^2, λ_1, λ_2, c, $\bar{\sigma}_x$, and $\bar{\sigma}_y$ in Eq. (39), one gets the value of the mass parameter m^2. Putting the $\bar{\sigma}_x$ and $\bar{\sigma}_y$ values in Eq. (28), one finds

$$h_x=f_\pi m_\pi^2 \quad \text{and} \quad h_y=\sqrt{2}f_K m_K^2-\frac{1}{\sqrt{2}}f_\pi m_\pi^2. \quad (40)$$

The Yukawa coupling gets fixed from the nonstrange constituent quark mass as $g=\frac{2m_u}{f_\pi}$. For $f_\pi=92.4$ MeV and the $m_u\sim 300.3$ MeV, one gets $g\sim 6.5$. The strange quark constituent mass becomes $m_s\sim 334.34$ MeV. The experimental value is $m_\eta=547.5$ MeV and $m_{\eta'}=957.78$ MeV. In Ref. [25], the parameter λ_2 is determined by taking $m_\eta=539$ MeV and $m_{\eta'}=963$ MeV as input because the sum of the squared masses $m_\eta^2+m_{\eta'}^2=(539)^2+(963)^2$ is almost equal to $(547.5)^2+(957.78)^2$, and the calculated parameters reproduce $m_\eta=539$ MeV and $m_{\eta'}=963$ MeV in the output.

III. RENORMALIZED POLYAKOV QUARK-MESON MODEL

Several of the recent QM/PQM model investigations with quark one-loop vacuum correction [52,53,57–68] have fixed the model parameters by the use of the curvature (or screening) masses of the π, K, η, η', and σ mesons where the pion decay constant has been identified as the vacuum expectation value of nonstrange condensate, and the vacuum strange condensate gets related to the pion and kaon decay

constant. However, it is well known that the physical masses are given by the poles of the meson propagators, and the residue of the pion propagator at its pole gets related to the pion decay constant [71–73]. Furthermore, the definition of the curvature mass of the meson involves the evaluation of its self-energy at the zero momentum [69,70,76,77] as one knows that the effective potential is the generator of the n-point functions of the theory at zero external momenta. Also one notes that the pole definition is the physical and gauge invariant one [74,75]. In the absence of the Dirac sea contributions, the pole mass becomes equivalent to the curvature mass for the model parameter fixing, but when the quark one-loop vacuum correction is present, the pole masses of the mesons become different from their screening masses [71,72]. In view of the above considerations, it becomes important to use the exact on-shell parameter fixing method for the renormalized Polyakov enhanced quark-meson (RPQM) model where the physical (pole) masses of the mesons, the pion, and kaon decay constants are put into the relation of the running mass parameter and couplings by using the on-shell and the minimal subtraction renormalization prescriptions [76,78,79]. In a very recent work [80], one of us has calculated the consistent effective potential and the on-shell renormalized parameters for the $2+1$ flavor quark-meson (QM) model where the quark one-loop vacuum fluctuation is properly renormalized. The calculation of the exact effective potential and the on-shell renormalization of the six parameters $m^2, \lambda_1, \lambda_2, c, h_x, h_y$ for the $2+1$ flavor RQM model are presented and reproduced in Appendix B.

Combining the RQM model vacuum effective potential with the thermal contributions of quarks-antiquarks and the Polyakov-loop potential, we write the grand thermodynamic potential of the RPQM model as the following:

$$\begin{aligned}\Omega_{\mathrm{RPQM}}(\Delta_x,\Delta_y,\Phi,\bar{\Phi},T,\mu) &= \frac{(m^2+m_{\mathrm{FIN}}^2)}{2}\left\{f_\pi^2\left(\frac{\Delta_x^2}{m_u^2}\right)+\frac{(2f_K-f_\pi)^2}{2}\left(\frac{\Delta_y^2}{m_s^2}\right)\right\}-(h_x+h_{x\mathrm{FIN}})f_\pi\left(\frac{\Delta_x}{m_u}\right)\\
&-(h_y+h_{y\mathrm{FIN}})\frac{(2f_K-f_\pi)}{\sqrt{2}}\left(\frac{\Delta_y}{m_s}\right)-\frac{(c+c_{\mathrm{FINTOT}})}{4}f_\pi^2(2f_K-f_\pi)\left(\frac{\Delta_x^2}{m_u^2}\right)\left(\frac{\Delta_y}{m_s}\right)\\
&+\frac{(\lambda_1+\lambda_{1\mathrm{FIN}})}{4}f_\pi^2(2f_K-f_\pi)^2\left(\frac{\Delta_x^2}{m_u^2}\right)\left(\frac{\Delta_y^2}{m_s^2}\right)+\frac{\{2(\lambda_1+\lambda_{1\mathrm{FIN}})+(\lambda_2+\lambda_{2\mathrm{FIN}})\}}{8}f_\pi^4\left(\frac{\Delta_x^4}{m_u^4}\right)\\
&+\frac{\{(\lambda_1+\lambda_{1\mathrm{FIN}})+(\lambda_2+\lambda_{2\mathrm{FIN}})\}}{16}(2f_K-f_\pi)^4\left(\frac{\Delta_y^4}{m_s^4}\right)+\frac{2N_c\Delta_x^4}{(4\pi)^2}\left[\frac{3}{2}-\ln\left(\frac{\Delta_x^2}{m_u^2}\right)-\mathcal{C}(m_\pi^2)\right.\\
&\left.-m_\pi^2\mathcal{C}'(m_\pi^2)\right]+\frac{N_c\Delta_y^4}{(4\pi)^2}\left[\frac{3}{2}-\ln\left(\frac{\Delta_y^2}{m_u^2}\right)-\mathcal{C}(m_\pi^2)-m_\pi^2\mathcal{C}'(m_\pi^2)\right]+\mathcal{U}(T,\Phi,\bar{\Phi})\\
&+\Omega_{q\bar{q}}(T,\mu;\Delta_x,\Delta_y,\Phi,\bar{\Phi}). \qquad (41)\end{aligned}$$

The expression $\Omega_{q\bar{q}}(T,\mu;\Delta_x,\Delta_y,\Phi,\bar{\Phi})$ is same as the $\Omega_{q\bar{q}}^{T,\mu}$ in Eq. (32) where $\bar{\sigma}_x$ and $\bar{\sigma}_y$ have been replaced by $\Delta_x=\frac{g\bar{\sigma}_x}{2}$ and $\Delta_y=\frac{g\bar{\sigma}_y}{\sqrt{2}}$. One gets the nonstrange constituent quark mass parameter Δ_x, strange constituent quark mass parameter Δ_y, Φ, and $\bar{\Phi}$ in the RPQM model by searching the global minimum of the grand potential in Eq. (41) for a given value of temperature T and chemical potential μ,

$$\frac{\partial\Omega_{\mathrm{RPQM}}}{\partial\Delta_x}=\frac{\partial\Omega_{\mathrm{RPQM}}}{\partial\Delta_y}=\frac{\partial\Omega_{\mathrm{RPQM}}}{\partial\Phi}=\frac{\partial\Omega_{\mathrm{RPQM}}}{\partial\bar{\Phi}}=0. \qquad (42)$$

In our calculations, we have used $m_\pi=138.0$ MeV, $m_K=496$ MeV. Here, in the RQM model, fixing the $m_\eta^2+m_{\eta'}^2=(547.5)^2+(957.78)^2$ and then taking the η mass as 527.58 MeV, one gets the η' mass equal to 968.89 MeV. The pole masses $m_\eta=527.58$ MeV and $m_{\eta'}=968.89$ MeV have been used for calculating the self-energy corrections (for η,η') and fixing of the parameters in the on-shell scheme because it has been checked that when the masses are calculated with the new set of renormalized parameters and respective self-energy corrections are added, the same pole masses are reproduced.

IV. RESULTS AND DISCUSSION

The nonstrange and strange direction chiral crossover transition and the confinement-deconfinement transition occurring on the temperature axis at $\mu=0$ are being explored here in detail. The pseudocritical temperature for the nonstrange, the strange chiral crossover transition, T_c^χ, T_c^s, and the confinement-deconfinement transition, T_c^Φ, are obtained by identifying the peaks in the respective temperature direction variation of the temperature derivative $\frac{\partial(\bar{\sigma}_x/\bar{\sigma}_{x0})}{\partial T}$, $\frac{\partial(\bar{\sigma}_y/\bar{\sigma}_{y0})}{\partial T}$, and $\frac{\partial\Phi}{\partial T}$.

Figures 1(a) and 1(b) show the respective temperature variations of the normalized nonstrange and strange chiral condensate at $\mu=0$ MeV and $m_\sigma=500$ MeV for the

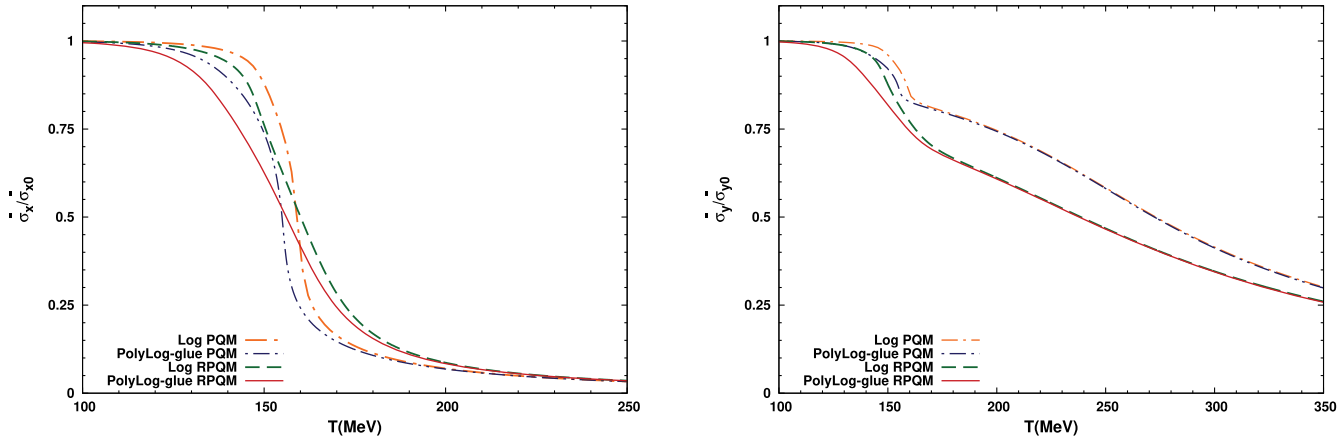

FIG. 1. Temperature variation of the $\bar{\sigma}_x/\bar{\sigma}_{x0}$ and the $\bar{\sigma}_y/\bar{\sigma}_{y0}$ for $m_\sigma = 500$ MeV at $\mu = 0$; $\bar{\sigma}_{x0} = f_\pi$ and $\bar{\sigma}_{y0} = \frac{2f_K - f_\pi}{\sqrt{2}}$. (a) Normalized nonstrange chiral condensate. (b) Normalized strange chiral condensate.

PQM and RPQM models with the Log and the PolyLog-glue forms of the Polyakov-loop potential. The term glue stands for the unquenching of the Polyakov-loop potential in the presence of the quark backreaction at $\mu = 0$. Though the temperature variation of the nonstrange condensate in the PolyLog-glue PQM model in Fig. 1(a) shifts early on the temperature scale due to the quark backreaction, it is sharper than that of the Log PQM model because the early occurring weaker deconfinement transition at $T_c^\Phi = 138.8$ MeV (from the Table IV) in the PolyLog-glue PQM model does not influence its chiral transition (at $T_c^\chi = 155.2$ MeV) that much while the Log PQM model relatively stronger deconfinement transition which occurs at $T_c^\Phi = 149.9$ MeV influences the chiral transition at $T_c^\chi = 159.3$ MeV. The above behavior can be inferred from the temperature variation of $\frac{\partial(\bar{\sigma}_x/\bar{\sigma}_{x0})}{\partial T}$ and $\frac{\partial\Phi}{\partial T}$ in the Log and the PolyLog-glue PQM models in Fig. 2(a). The temperature variation of the nonstrange condensate becomes significantly smoother due to the quark one-loop vacuum correction in the Log RPQM model as shown Fig. 1(a), and it also gets influenced by Log form of the Polyakov-loop potential which causes a stronger deconfinement transition. The sharper temperature variation of $\frac{\partial\Phi}{\partial T}$ and its peak at $T_c^\Phi = 148.1$ MeV have a strong influence on the chiral transition because the $\frac{\partial(\bar{\sigma}_x/\bar{\sigma}_{x0})}{\partial T}$ temperature variation peaks at the adjacent $T_c^\chi = 148.9$ MeV and develops a small very slowly decreasing shoulder-like structure thereafter (falling short of developing the second peak) in Fig. 2(b). Therefore, the finding of T_c^χ has an in-built ambiguity of $\sim +9.0$ MeV. Due to the combined effect of the quark one-loop vacuum correction and the quark backreaction, one gets most smooth temperature variation of the nonstrange condensate in Fig. 1(a) for the PolyLog-glue RPQM model. The temperature variation of $\frac{\partial\Phi}{\partial T}$ is very smooth and well separated from the quite

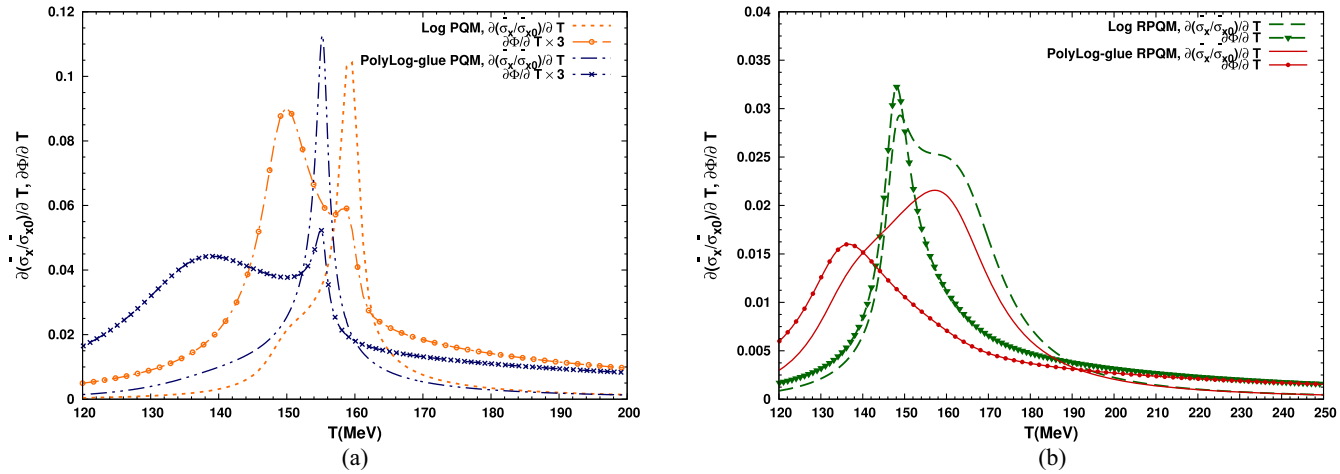

FIG. 2. Temperature variation of $\frac{\partial\bar{\sigma}_x/\bar{\sigma}_{x0}}{\partial T}$ and $\frac{\partial\Phi}{\partial T}$ for $m_\sigma = 500$ MeV at $\mu = 0$. (a) Results for the Log and PolyLog-glue PQM model. (b) Results for the Log and PolyLog-glue RPQM model.

TABLE III. Parameters of the different model scenarios. The RQM model parameters are obtained by putting $\Lambda = \Lambda_0$ in Eqs. (B80)–(B85).

Model	m_σ (MeV)	λ_2	$c(\mathrm{MeV}^2)$	λ_1	$m^2(\mathrm{MeV}^2)$	$h_x(\mathrm{MeV}^3)$	$h_y(\mathrm{MeV}^3)$
QM	400	46.43	4801.82	−5.89	$(494.549)^2$	$(120.73)^3$	$(336.43)^3$
	500	46.43	4801.82	−2.69	$(434.305)^2$	$(120.73)^3$	$(336.43)^3$
	600	46.43	4801.82	1.141	$(342.139)^2$	$(120.73)^3$	$(336.43)^3$
RQM	400	34.88	7269.20	1.45	$(442.447)^2$	$(119.53)^3$	$(323.32)^3$
	500	34.88	7269.20	3.676	$(396.075)^2$	$(119.53)^3$	$(323.32)^3$
	600	34.88	7269.20	8.890	$(256.506)^2$	$(119.53)^3$	$(323.32)^3$

smooth temperature variation of $\frac{\partial(\bar{\sigma}_x/\bar{\sigma}_{x0})}{\partial T}$ in Fig. 2(b), and the deconfinement transition occurs early as $\frac{\partial\Phi}{\partial T}$ temperature variation peaks at $T_c^\Phi = 136.6$ MeV while the temperature variation of $\frac{\partial(\bar{\sigma}_x/\bar{\sigma}_{x0})}{\partial T}$ peaks later giving $T_c^\chi = 157.3$ MeV.

Strange condensate temperature variations for both the Log and PolyLog-glue PQM models have a small and sharp kink-like structure near the nonstrange chiral transition temperature T_c^χ in Fig. 1(b). The above kink-like structure gets smoothed out and hence disappears due to effect of quark one-loop vacuum correction in the RPQM model. The quark backreaction present in the PolyLog-glue PQM model causes a noticeable decrease in the strange condensate in the temperature range 120 to 165 MeV. After $T > 165$ MeV, the strange condensate temperature variation for the PolyLog-glue PQM model becomes degenerate with that of the Log PQM model. Note that the strange direction explicit symmetry breaking strength h_y (see Table III) becomes weaker by a relatively large amount (in comparison to h_x) as the kaon curvature mass $m_{K,c} = 467.99$ MeV becomes smaller than its pole mass $m_K = 496$ MeV after renormalization of the parameters in the RPQM model. Hence, the melting of the strange condensate gets significantly enhanced due to the effect of quark one-loop vacuum correction in the RPQM model. For the temperature ranging from 110 to 185 MeV in the vicinity of the nonstrange chiral crossover transition temperature (T_c^χ), the melting of the strange condensate in the Log RPQM model differs significantly from its largest melting noticed in the PolyLog-glue RPQM model in Fig. 1(b). The strange condensate temperature variation for the Log and PolyLog-glue RPQM models merge with each other for $T > 180$ MeV. The earliest chiral transition in the strange direction occurs in the Log RPQM model at $T_c^s = 225.6$ MeV while the strange direction chiral transition for the Log PQM model occurs at the $T_c^s = 252.1$ MeV. Table IV summarizes the $\mu = 0$ transition pseudocritical temperatures T_c^χ, T_c^s, and T_c^Φ for $m_\sigma = 400$, 500, and 600 MeV in the PQM and RPQM models with the Log and PolyLog-glue forms of the Polyakov-loop potential.

The lattice data cannot be directly compared with the temperature variations of the nonstrange and strange condensate, $\langle\bar{\sigma}_x\rangle$ and $\langle\bar{\sigma}_y\rangle$. A suitable combination of the light and strange quark condensates is calculated to eliminate the quadratic divergences in the linear quark mass dependent correction to the chiral condensate. The above quantity is further normalized by the corresponding combination of condensates calculated at $T = 0$ MeV [14]. Thus, one finds the chiral symmetry breaking order parameter called the subtracted chiral condensate $\Delta_{l,s}(T)$ as given below,

$$\Delta_{l,s}(T) = \frac{\langle\bar{\sigma}_x\rangle(T) - (\frac{h_x}{h_y})\langle\bar{\sigma}_y\rangle(T)}{\langle\bar{\sigma}_x\rangle(0) - (\frac{h_x}{h_y})\langle\bar{\sigma}_y\rangle(0)}. \tag{43}$$

The subtracted chiral condensate temperature variations (at $\mu = 0$) have been calculated for the PQM and RPQM models with the Log and PolyLog-glue forms of the Polyakov-loop potential and compared with the Wuppertal-Budapest Collaboration lattice QCD (WBLQCD-I) data of Δ_{ls} [102] in Fig. 3(a). We find that the calculation of the Δ_{ls} temperature variation in our PolyLog-glue RPQM model gives the closest fit to the WBLQCD-I data. Figure 3(b)

TABLE IV. Pseudocritical temperatures at $\mu = 0$.

		$m_\sigma = 400$ MeV			$m_\sigma = 500$ MeV			$m_\sigma = 600$ MeV		
Polyakov loop	Models	T_c^χ (MeV)	T_c^s (MeV)	T_c^Φ (MeV)	T_c^χ (MeV)	T_c^s (MeV)	T_c^Φ (MeV)	T_c^χ (MeV)	T_c^s (MeV)	T_c^Φ (MeV)
Log	PQM	149.5	244.3	149.5	159.3	252.1	149.9	171.9	261.7	150.5
	RPQM	146.4	222.8	146.0	148.9	225.6	148.1	181.1	233.8	150.1
PolyLog-glue	PQM	142.5	245.1	142.4	155.2	252.3	138.8	169.5	261.2	129.1
	RPQM	145.6	225.6	133.6	157.3	227.8	136.6	179.6	235.3	138.6

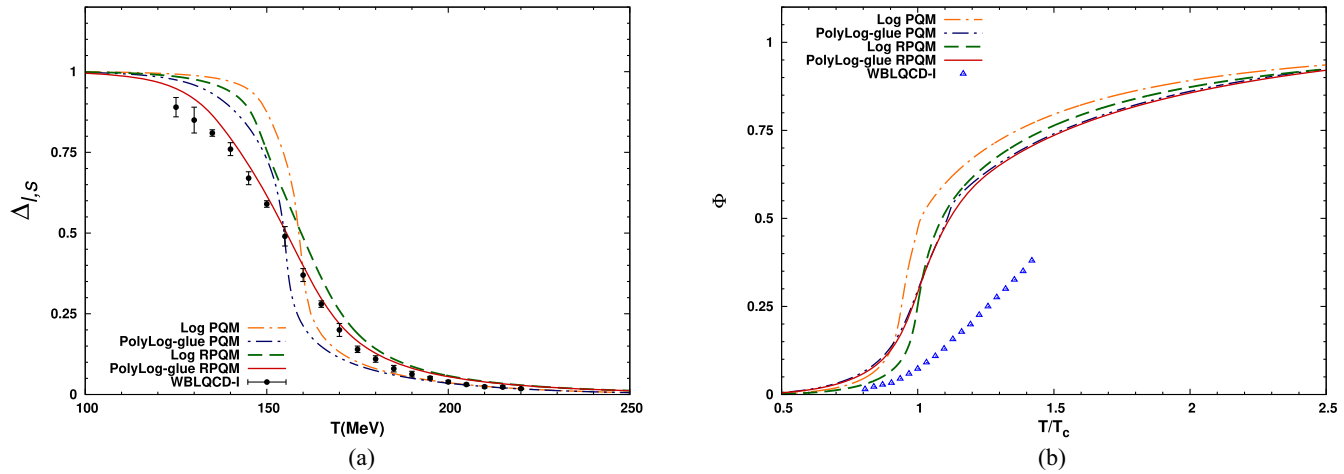

FIG. 3. Temperature variation of Δ_{ls} and Φ for $m_\sigma = 500$ MeV at $\mu = 0$. The lattice data of WBLQCD-I for Δ_{ls} and Φ have been taken from Ref. [102] in the continuum limit. (a) Subtracted chiral condensate Δ_{ls}. (b) The Polyakov-loop order parameter Φ.

presents the comparison of the WBLQCD-I Collaboration data [102] for the reduced temperature scale variation of the Polyakov loop with the temperature variation of the Polyakov-loop condensate obtained in the PQM and RPQM model calculations having the Log and PolyLog-glue forms for the Polyakov-loop potential. The WBLQCD-I [102] data for the Polyakov loop lie significantly below the temperature variation of the Polyakov-loop condensate that one finds in the all model calculations.

A. Comparison of thermodynamic quantities with the lattice QCD data

We compare the thermodynamic quantities pressure, entropy density, energy density, specific heat, and speed of sound in the PQM model and the RPQM model with the Log and PolyLog-glue forms of the Polyakov-loop potential. It is well documented in the literature [58–61,79,80,95] that the curvature mass based parameter fixing of the model in the presence of the quark one-loop vacuum fluctuation gives rise to an excessively soft and smooth chiral transition. Therefore, in order to make quantitative comparisons with the results obtained from the on-shell renormalized RPQM model, we have presented the plots of the thermodynamic quantities also for the Polyakov-loop augmented quark-meson model with vacuum term (PQMVT) where the model parameters are fixed by the use of curvature masses, and the PolyLog-glue form of the Polyakov-loop potential has been taken. The effective potential (for the chiral part) given in Refs. [64,80] for the PQMVT model has been used to calculate the thermodynamic quantities. It is to be noted that the effective potential of the curvature mass parametrized PQMVT model differs from the on-shell RPQM model, only in the vacuum part ($T = 0$, $\mu = 0$) that represents the physics of chiral symmetry.

The QCD phase transition has a strong influence on these thermodynamic quantities. The pressure of a QCD system can be defined as negative of the grand potential,

$$P(T,\mu) = -\Omega(T,\mu), \tag{44}$$

and the pressure is normalized to zero in the vacuum, i.e., $P(0,0) = 0$.

The reduced temperature scale variation of the pressure for the PolyLog-glue RPQM model (where the quark backreaction and the quark one-loop vacuum correction, both are present) in Fig. 4 stands close to the lattice QCD data of the pressure that have been reported by the WBLQCD-II [103] and HotQCD-I [104] Collaborations. The pressure variation in the PolyLog-glue PQMVT model is significantly different from that of the RPQM model result. Here, it is worthwhile to mention that the $\mu = 0$ axis

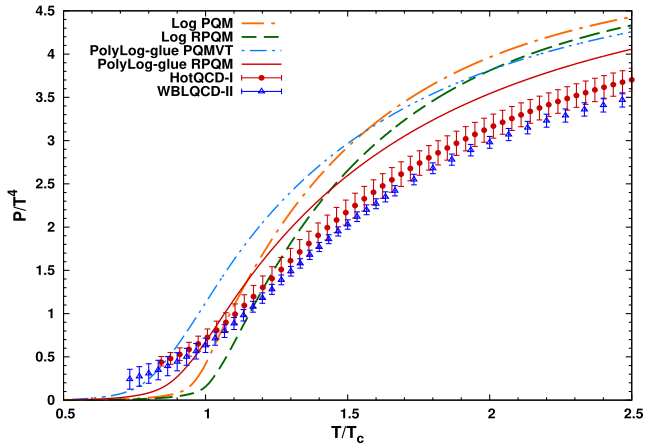

FIG. 4. Temperature variation of the pressure for $m_\sigma = 500$ MeV at $\mu = 0$. The lattice data of the pressure, in the continuum limit of HotQCD-I and WBLQCD-II, have been taken from Refs. [104,103], respectively.

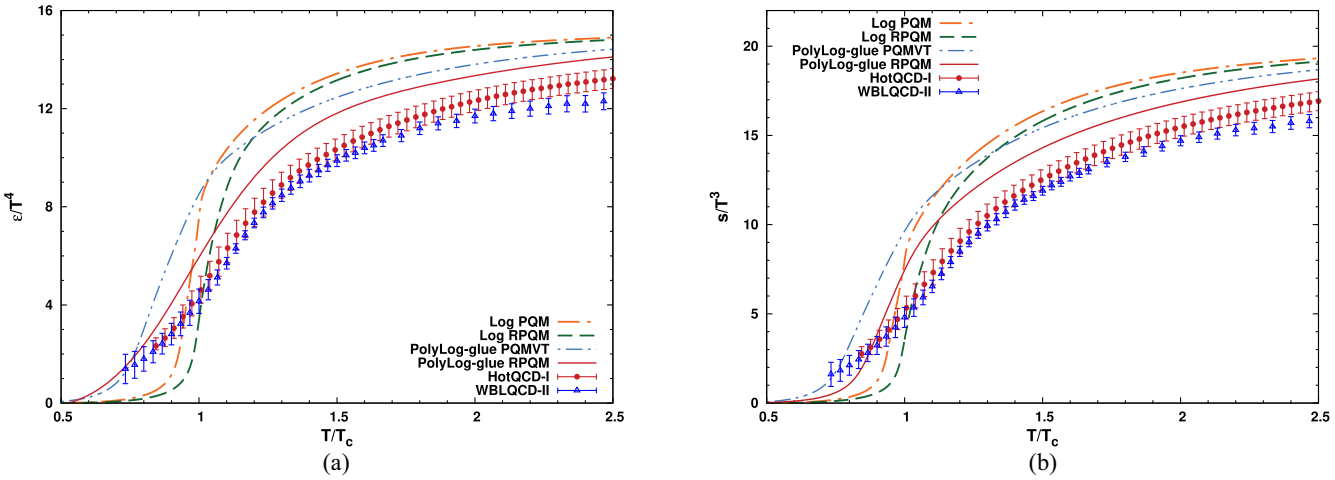

FIG. 5. Temperature variation of the energy density and entropy density for $m_\sigma = 500$ MeV at $\mu = 0$. The lattice data of the energy density and entropy density, in the continuum limit of HotQCD-I and WBLQCD-II, have been taken from Refs. [104,103], respectively. (a) Energy density. (b) Entropy density.

chiral crossover transition temperature $T_c^\chi = 177.8$ MeV for the PQMVT model while $T_c^\chi = 157.3$ MeV for the RPQM model.

In order to find the thermodynamic quantities other than pressure, one needs to take the temperature derivative of the grand potential. The entropy density s, the energy density ϵ, and the interaction measure Δ at the zero quark chemical potential are defined by

$$s = -\frac{\partial \Omega}{\partial T}, \tag{45}$$

$$\epsilon = -P + Ts, \tag{46}$$

$$\Delta = \epsilon - 3P. \tag{47}$$

The respective temperature variations of the energy density and the entropy density in Figs. 5(a) and 5(b), either in the PQM or RPQM models with the Log form of the Polyakov-loop potential, increase very rapidly near T_c and attain saturation after the temperature 1.5 T_c. The lattice QCD data of the WBLQCD-II [103] and HotQCD-I [104] Collaborations for the energy density (entropy density) temperature variations in Fig. 5(a) [Fig. 5(b)], apart from being close to the energy density (entropy density) obtained from the PolyLog-glue RPQM model computation, show quite a similar rising pattern on the reduced temperature scale. The energy density and entropy density temperature variations obtained from the PolyLog-glue PQMVT model are significantly different from those of the RPQM model.

The interaction measure is found to have highest rising temperature variation for the Log PQM model in Fig. 6(a).

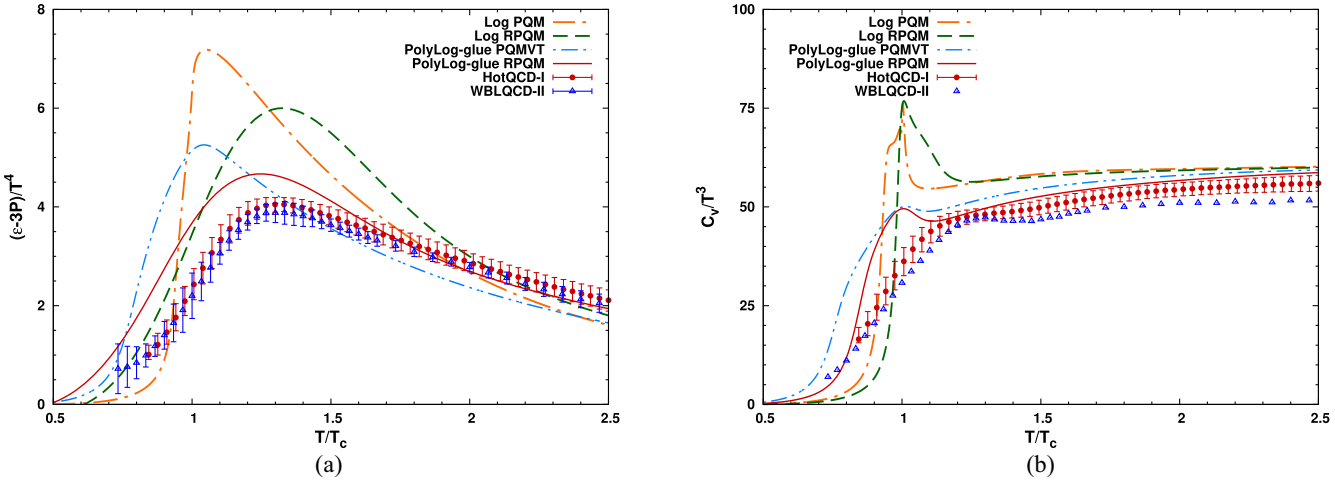

FIG. 6. Temperature variation of the interaction measure and specific heat for $m_\sigma = 500$ MeV at $\mu = 0$. The lattice data of the interaction measure and specific heat, in the continuum limit of HotQCD-I and WBLQCD-II, have been taken from Refs. [103,104], respectively. (a) Interaction measure. (b) Specific heat.

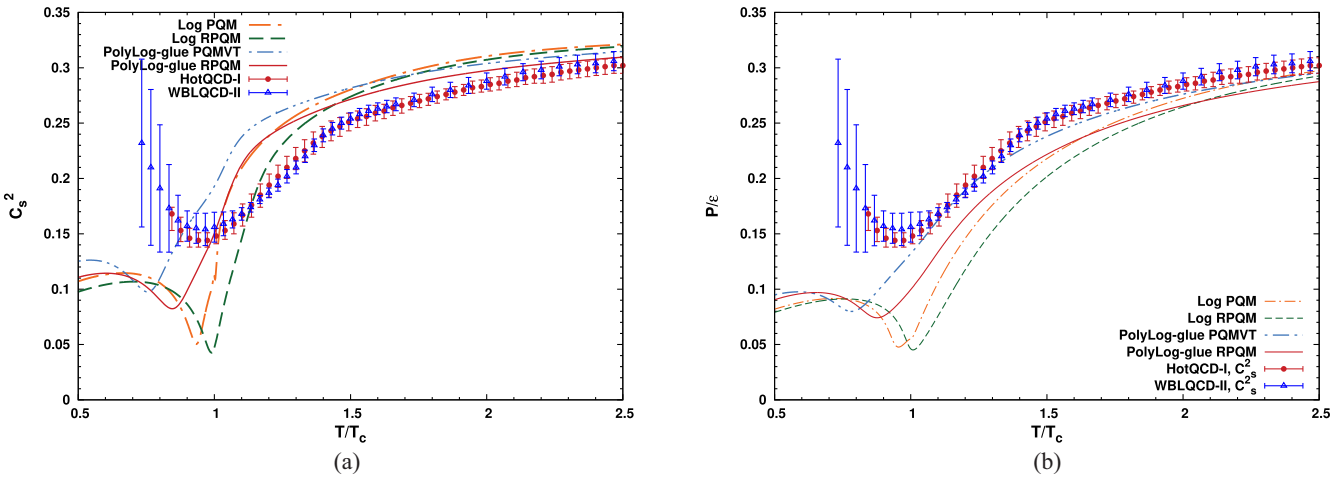

FIG. 7. Temperature variation of C_s^2 and P/ϵ for $m_\sigma = 500$ MeV at $\mu = 0$. The lattice data of C_s^2, in the continuum limit of HotQCD-I and WBLQCD-II, have been taken from Refs. [103,104], respectively. In (b), model calculations of P/ϵ have been compared with the lattice data of C_s^2. Here, $T_c = T_c^\chi$. (a) Squared speed of sound (C_s^2). (b) Ratio of pressure with energy.

When the quark backreaction and the quark one-loop vacuum correction both are present in the PolyLog-glue RPQM model, the calculated temperature variation of the interaction measure with a significantly reduced height shows quite a close resemblance in its pattern with the latest lattice data for the temperature variation of the interaction measure (also lattice data for $T > 1.5T_c$ has a good match with the theoretical calculation) reported by the WBLQCD-II [103] and HotQCD-I [104] Collaborations. The temperature variation of the interaction measure calculated in the PQMVT model is also significantly different from that of the RPQM model result.

The expression for the specific heat capacity at constant volume is written as

$$C_V = \left.\frac{\partial\epsilon}{\partial T}\right|_V = -T\left.\frac{\partial^2\Omega}{\partial T^2}\right|_V. \tag{48}$$

The specific heat (normalized with T^3) variation on the reduced temperature scale in Fig. 6(b) shows the highest and sharpest peak near T_c in the Log PQM model which becomes smoother in the Log RPQM model. The quark one-loop vacuum correction in the presence of the quark backreaction in the PolyLog-glue RPQM model gives rise to a most smooth temperature variation of the specific heat that has a well rounded peak structure. The above-mentioned pattern has a close resemblance with the specific heat temperature variation reported in the WBLQCD-II [103] and HotQCD-I [104] lattice data. Furthermore, the PolyLog-glue RPQM model calculation of the specific heat temperature variation for the $T > 1.1T_c$ matches very well with the said lattice data for the specific heat. The temperature variation of the specific heat computed from the PQMVT model shows noticeable difference from that of the RPQM model result.

In the strongly interacting medium, the speed of sound is a very important quantity, and at fix entropy density s, the square of the speed of sound is define by

$$C_s^2 = \left.\frac{\partial P}{\partial\epsilon}\right|_s = \left.\frac{\partial P}{\partial T}\right|_V \Big/ \left.\frac{\partial\epsilon}{\partial T}\right|_V = \frac{s}{C_V}. \tag{49}$$

The reduced temperature scale variations of C_s^2 (P/ϵ) in Fig. 7(a) [Fig. 7(b)], for the Log PQM as well as RPQM and PolyLog-glue RPQM as well as PQMVT models, are compared with the WBLQCD-II [103] and HotQCD-I [104] lattice data. The C_s^2 temperature variation pattern of the PolyLog-glue RPQM model in Fig. 7(a) being noticeably different from that of the PQMVT model result resembles closely the rising trend of C_s^2 that one observes in the lattice QCD data, and agreement between the results become quite good after $T > 1.4T_c$ when the lattice data approaches the PolyLog-glue RPQM model result from below. The lattice data for the temperature variation of C_s^2 in its lower bound matches well with the P/ϵ temperature variation that has been calculated from the curvature mass parametrized PolyLog-glue PQMVT model for $T > 1.1T_c$ while it lies just above the P/ϵ temperature variations which have been computed in other model scenarios.

B. Illustration of the phase diagrams and their CEP positions

The phase diagrams of the PQM and RPQM models with the Log and PolyLog-glue forms of the Polyakov-loop potential are presented in Figs. 8–10, respectively, for $m_\sigma = 400$, 500, and 600 MeV. Table V presents a comparison of the positions of CEP in different model scenarios. In Fig. 8 for $m_\sigma = 400$ MeV and $T_0 = 187$ MeV, the PQM model CEP position at $(T_{\rm CEP}, \mu_{\rm CEP}) = (149.0, 26.4)$ MeV $\{(T_{\rm CEP}, \mu_{\rm CEP}) = (138.5, 61.1)$ MeV$\}$

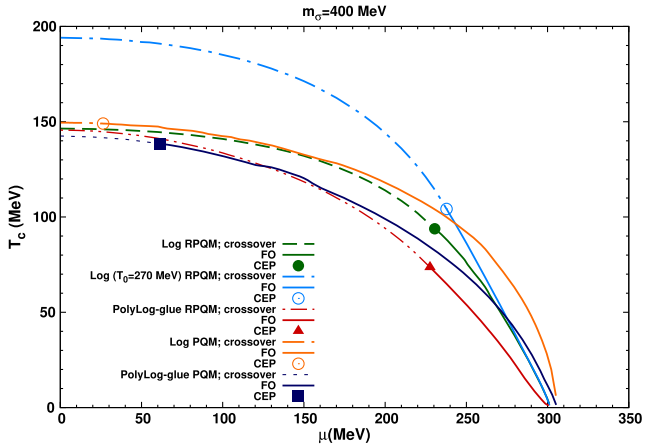

FIG. 8. Phase diagrams for $m_\sigma = 400$ MeV.

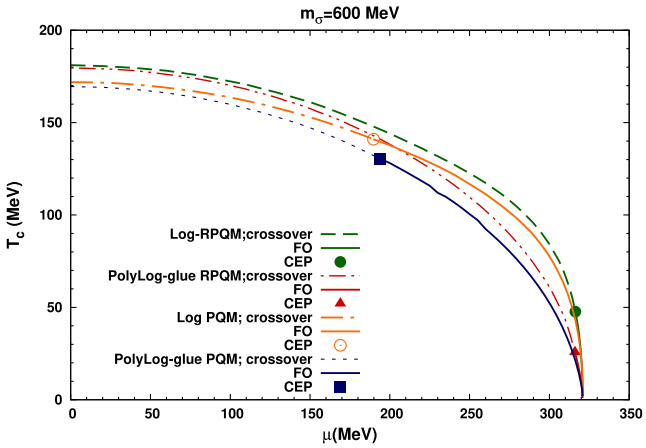

FIG. 10. Phase diagrams for $m_\sigma = 600$ MeV.

for the Log {PolyLog-glue} Polyakov-loop potential shifts to the position $(T_{\mathrm{CEP}}, \mu_{\mathrm{CEP}}) = (93.8, 230.5)$ MeV $\{(T_{\mathrm{CEP}}, \mu_{\mathrm{CEP}}) = (73.6, 227.6)\,\mathrm{MeV}\}$ in the Log {PolyLog-glue} RPQM model due to the quark one-loop vacuum correction. Comparing the CEP of the Log RPQM model with that of the PolyLog-glue RPQM model, we find that the CEP moves down in the temperature direction by 20.2 MeV due to the effect of the quark backreaction in the PolyLog-glue RPQM model while it shifts leftward on the chemical potential axis by a small amount (only 2.9 MeV). In contrast to the above explained behavior, the temperature down shift in the PolyLog-glue PQM model CEP position is only 10.5 MeV when compared to the CEP of the Log PQM model while its position in the chemical potential direction increases (moves right) by 34.7 MeV. Our RPQM model result shows the confirmation of Ref. [99] observation that the quark backreaction due to the unquenching of the Polyakov-loop potential links the chiral and deconfinement phase transition also at small temperature and large chemical potential. One also finds

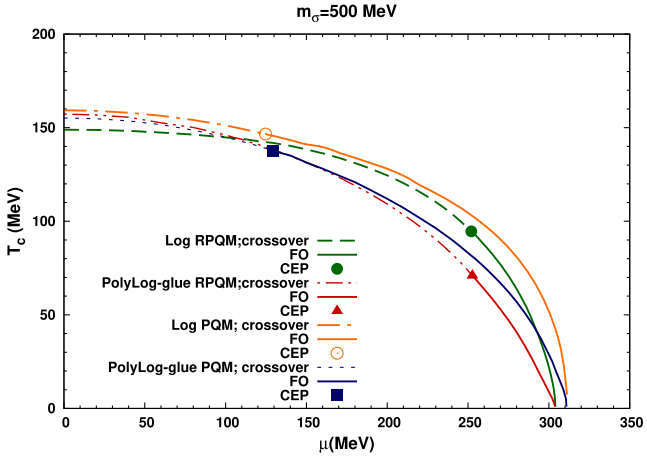

FIG. 9. Phase diagrams for $m_\sigma = 500$ MeV.

that the curvature of the phase transition line increases due to the above effect.

We point out that when the quark one-loop vacuum correction is added to the effective potential of the QM model, and the curvature masses of the mesons are used to fix the model parameters as in Refs. [58–61], the calculated shift in the position of the CEP is quite large and overestimated as reported in our recent 2 and $2+1$ flavor renormalized quark-meson model investigations [79,80,95] where the consistent and exact parameter fixings have been done using the on-shell method. After including the quark one-loop vacuum correction and fixing the model parameters by the use of curvature masses of the mesons, Schaefer *et al.* [59], in their $2+1$ flavor PQM model work with the Log Polyakov-loop potential whose parameter $T_0 = 270$ MeV (for the Pure Yang-Mills $SU_c(3)$ gauge theory), find the CEP at $(T_{\mathrm{CEP}}, \mu_{\mathrm{CEP}}) = (90.0, 283.0)$ MeV when $m_\sigma = 400$ MeV. It is worth emphasizing that if we take the Log Polyakov-loop potential parameter $T_0 = 270$ MeV in our on-shell parameterized $2+1$ flavor RPQM model, we find that in our calculation, the CEP coordinate $(T_{\mathrm{CEP}}, \mu_{\mathrm{CEP}}) = (104.23, 237.8)$ MeV lies at quite a higher up position in the temperature direction by 14.23 MeV, having also a significantly robust chemical potential direction shift of 45.2 MeV toward the left in the phase diagram, when it is compared with the corresponding phase diagram given in Fig. 1(b) of Ref. [59].

When m_σ increases from 400 to 500 MeV in Fig. 9, the CEP moves rightward on the chemical potential axis. We find that when $m_\sigma = 500$ MeV, the CEP in the PQM model at $(T_{\mathrm{CEP}}, \mu_{\mathrm{CEP}}) = (146.6, 124.7)\{(137.7, 129.6)\}$ MeV for the Log {PolyLog-glue} Polyakov-loop potential moves to the position $(T_{\mathrm{CEP}}, \mu_{\mathrm{CEP}}) = (94.6, 252.0)\{(70.9, 252.7)\}$ MeV in the Log {PolyLog-glue} RPQM model. Comparing the CEP of the Log RPQM model with that of the PolyLog-glue RPQM model, one notes that here for the $m_\sigma = 500$ MeV case, the CEP moves down in temperature by a larger amount of 23.7 MeV (compared to the

TABLE V. Critical end points.

		$m_\sigma = 400$ MeV	$m_\sigma = 500$ MeV	$m_\sigma = 600$ MeV
Polyakov loop	Models	$(T_{\rm CEP}, \mu_{\rm CEP})$ MeV	$(T_{\rm CEP}, \mu_{\rm CEP})$ MeV	$(T_{\rm CEP}, \mu_{\rm CEP})$ MeV
Log	PQM	(149.0, 26.4)	(146.6, 124.7)	(141.0, 189.8)
	RPQM	(93.8, 230.5)	(94.6, 252.0)	(47.7, 316.3)
	RPQM ($T_0 = 270$ MeV)	(104.23, 237.8)	…	…
PolyLog-glue	PQM	(138.5, 61.1)	(137.7, 129.6)	(130.4, 193.9)
	RPQM	(73.6, 227.6)	(70.9, 252.7)	(25.7, 316.1)

$m_\sigma = 400$ MeV) due to the effect of the quark backreaction while its rightward shift in the chemical potential direction is negligibly small (only 0.7 MeV). In contrast, the temperature down shift in the PolyLog-glue PQM model CEP position is only 8.9 MeV when compared to the CEP of the Log PQM model while its position in the chemical potential direction shifts rightward by 4.9 MeV. Here, also we find that the curvature of the phase transition line increases due to the quark backreaction as in Ref. [99].

The PQM model CEP at $(T_{\rm CEP}, \mu_{\rm CEP}) = (141.0, 189.8)\{(130.4, 193.9)\}$ MeV when the $m_\sigma = 600$ MeV in Fig. 10, for the Log {PolyLog-glue} Polyakov-loop potential moves to the position $(T_{\rm CEP}, \mu_{\rm CEP}) = (47.7, 316.3)\{(25.7, 316.1)\}$ MeV in the Log {PolyLog-glue} RPQM model. Here, for $m_\sigma = 600$ MeV also, the Log RPQM model CEP shifts, vertically down on the temperature axis by 22.0 MeV due to the unquenching of the Polyakov-loop potential while the chemical potential is almost the same. Here, it is relevant to emphasize that we are getting a well placed CEP in the phase diagram of the RPQM model even for the case of $m_\sigma = 600$ MeV while the curvature mass parametrization of the PQM model with the quark one-loop vacuum correction generates such an excessively large soothing effect on the chiral phase transition that the CEP altogether disappears from the phase diagram, and one gets a complete chiral crossover transition in the entire $\mu - T$ plane as reported in Refs. [58–60].

V. SUMMARY AND CONCLUSION

The consistent and improved chiral effective potential of the renormalized 2 + 1 flavor quark-meson model (RQM), whose parameters are fixed on-shell after the inclusion of quark one-loop vacuum correction, has been augmented with the different forms of the Polyakov-loop potential with and without quark backreaction. The resulting quantum chromodynamics (QCD)-like framework of the 2 + 1 flavor renormalized Polykov quark-meson (RPQM) model has been used to investigate the interplay of the chiral symmetry restoring and the deconfinement phase transitions. The results have been compared with the PQM model where the fermionic vacuum fluctuations are neglected. The temperature variation of the thermodynamics quantities, pressure, entropy density, energy density, interaction measure, specific heat, speed of sound, and the ratio P/ϵ, have been computed at $\mu = 0$ MeV and compared with the latest 2 + 1 flavor lattice data of the Wuppertal-Budapest and HotQCD Collaborations [103,104]. The thermodynamics quantities computed for the on-shell parameterized RPQM model have been compared with the corresponding calculations in the curvature mass parametrized PQMVT model where the PolyLog-glue form of the Polyakov-loop potential has been used in both the cases to account for the quark backreaction. The PQM and RPQM model phase diagrams for $m_\sigma = 400$, 500, 600 MeV have been computed and compared with/without the quark backreaction in the Polyakov-loop potential.

The most smooth temperature variation of the nonstrange chiral condensate is observed for the PolyLog-glue RPQM model. Since the strange direction explicit symmetry breaking strength h_y is reduced by a relatively large amount after renormalization, the melting of the strange condensate is significantly large in the RPQM model. The temperature variation of the subtracted chiral condensate Δ_{ls} calculated in the PolyLog-glue RPQM model at $\mu = 0$, and $m_\sigma = 500$ MeV shows the best agreement with the WBQCD-I lattice data of Δ_{ls}.

The recent WBLQCD-II [103] and HotQCD-I [104] lattice data for the pressure, entropy density, and energy density are quite close to their respective temperature variation that we obtain in our PolyLog-glue RPQM model calculation. The interaction measure peak is smallest in its PolyLog-glue RPQM model temperature variation and agrees well with the WBLQCD-II [103] and HotQCD-I [104] LQCD data for $T > 1.5T_c$. The very smooth and rounded peak noticed in the specific heat temperature variation of the lattice QCD data has quite a close resemblance with our PolyLog-glue RPQM results. The C_s^2 [103,104] temperature variation calculated from the PolyLog-glue RPQM model is quite close to the lattice QCD data for C_s^2. The temperature variations of the thermodynamic quantities obtained using the curvature mass-based parametrization in the PQMVT model (for the PolyLog-glue form of the Polyakov-loop potential) differ significantly from the corresponding temperature variations calculated by the use of the consistent on-shell parametrization in the RPQM model. The lower bound of the lattice QCD data for the C_s^2 temperature variation

matches with the PolyLog-glue PQMVT model temperature variation of the ratio P/ϵ for $T > 1.1T_c$.

The CEP of the Log RPQM model moves significantly down ($\Delta T_{\rm CEP} = 20.2$–$23.7$ MeV) on the temperature axis due to the presence of the quark backreaction in the PolyLog-glue RPQM model while the shift in the chemical potential direction is negligible. This finding confirms the observation of Ref. [99] that unquenching of the Polyakov-loop potential links the chiral and deconfinement phase transitions at all temperatures and chemical potentials. We point out that the smoothing effect of the quark one-loop vacuum correction on the chiral transition phase boundary is excessively large and overestimated in the earlier investigations [59,60] where the curvature masses of the mesons have been used for fixing the model parameters while the f_π and f_K are taken as constant. In these studies, one gets a very large crossover and a smaller first order region. Therefore, the CEP gets located in the right-most lower corner of the $\mu - T$ plane at smaller temperatures and very high chemical potentials. We emphasize that the smoothing effect of the quark one-loop vacuum correction becomes moderate in our consistent on-shell parametrized RPQM model studies because we find a comparatively larger first order region in the $\mu - T$ plane of the phase diagram for $m_\sigma = 400$ and 500 MeV, and therefore, the CEP moves higher up in the phase diagram toward the temperature axis. Note that we are getting a well placed CEP in the phase diagram of the RPQM model even for the case of $m_\sigma = 600$ MeV while the CEP altogether disappears, and one gets a complete chiral crossover transition in the entire $\mu - T$ plane of the phase diagram reported in the studies [59,60] where the quark one-loop vacuum correction is included in the PQM model but the parameters are fixed using the curvature masses of the mesons.

APPENDIX A: INTEGRALS

The divergent loop integrals are regularized by incorporating dimensional regularization,

$$\int_p = \left(\frac{e^{\gamma_E}\Lambda^2}{4\pi}\right)^\epsilon \int \frac{d^d p}{(2\pi)^d}, \tag{A1}$$

where $d = 4 - 2\epsilon$, γ_E is the Euler-Mascheroni constant, and Λ is the renormalization scale associated with the $\overline{\rm MS}$ scheme,

$$\mathcal{A}(m_f^2) = \int_p \frac{1}{p^2 - m_f^2} = \frac{i m_f^2}{(4\pi)^2}\left[\frac{1}{\epsilon} + 1 + \ln(4\pi e^{-\gamma_E}) + \ln\left(\frac{\Lambda^2}{m_f^2}\right)\right].$$

We rewrite this after redefining $\Lambda^2 \to \Lambda^2 \frac{e^{\gamma_E}}{4\pi}$,

$$\mathcal{A}(m_f^2) = \frac{i m_f^2}{(4\pi)^2}\left[\frac{1}{\epsilon} + 1 + \ln\left(\frac{\Lambda^2}{m_f^2}\right)\right], \tag{A2}$$

$$\mathcal{B}(p^2, m_f) = \int_k \frac{1}{(k^2 - m_f^2)[(k+p)^2 - m_f^2)]} = \frac{i}{(4\pi)^2}\left[\frac{1}{\epsilon} + \ln\left(\frac{\Lambda^2}{m_f^2}\right) + \mathcal{C}(p^2, m_f)\right], \tag{A3}$$

$$\mathcal{B}'(p^2, m_f) = \frac{i}{(4\pi)^2}\mathcal{C}'(p^2, m_f), \tag{A4}$$

$$\mathcal{C}(p^2, m_f) = 2 - 2\sqrt{\frac{4m_f^2}{p^2} - 1}\arctan\left(\frac{1}{\sqrt{\frac{4m_f^2}{p^2} - 1}}\right); \qquad \mathcal{C}'(p^2, m_f) = \frac{4m_f^2}{p^4\sqrt{\frac{4m_f^2}{p^2} - 1}}\arctan\left(\frac{1}{\sqrt{\frac{4m_f^2}{p^2} - 1}}\right) - \frac{1}{p^2}, \tag{A5}$$

$$\mathcal{C}(p^2, m_f) = 2 + \sqrt{1 - \frac{4m_f^2}{p^2}}\ln\left(\frac{1 - \sqrt{1 - \frac{4m_f^2}{p^2}}}{1 + \sqrt{1 - \frac{4m_f^2}{p^2}}}\right); \qquad \mathcal{C}'(p^2, m_f) = \frac{2m_f^2}{p^4\sqrt{\frac{4m_f^2}{p^2} - 1}}\ln\left(\frac{1 - \sqrt{1 - \frac{4m_f^2}{p^2}}}{1 + \sqrt{1 - \frac{4m_f^2}{p^2}}}\right) - \frac{1}{p^2}. \tag{A6}$$

Equations (A5) and (A6) are valid with the constraints ($p^2 < 4m_f^2$) and ($p^2 > 4m_f^2$), respectively,

$$\mathcal{B}(p^2, m_u, m_s) = \int_k \frac{1}{(k^2 - m_s^2)[(k+p)^2 - m_u^2)]} = \frac{i}{(4\pi)^2}\left[\frac{1}{\epsilon} + \ln\left(\frac{\Lambda^2}{m_u^2}\right) + \mathcal{C}(p^2, m_u, m_s)\right], \tag{A7}$$

$$\mathcal{C}(p^2, m_u, m_s) = 2 - \frac{1}{2}\left[1 + \frac{m_s^2 - m_u^2}{p^2}\right]\ln\left(\frac{m_s^2}{m_u^2}\right) - \frac{\mathcal{G}(p^2)}{p^2}\left[\arctan\left(\frac{p^2 - m_s^2 + m_u^2}{\mathcal{G}(p^2)}\right) + \arctan\left(\frac{p^2 + m_s^2 - m_u^2}{\mathcal{G}(p^2)}\right)\right], \tag{A8}$$

$$\mathcal{G}(p^2) = \sqrt{\{(m_s+m_u)^2 - p^2\}\{p^2 - (m_s-m_u)^2\}}, \tag{A9}$$

$$\mathcal{C}'(p^2, m_u, m_s) = \frac{m_s^2 - m_u^2}{2p^4}\ln\left(\frac{m_s^2}{m_u^2}\right) + \frac{p^2(m_s^2+m_u^2) - (m_s^2-m_u^2)^2}{p^4\mathcal{G}(p^2)}\left[\arctan\left(\frac{(p^2 - m_s^2 + m_u^2)}{\mathcal{G}(p^2)}\right) + \arctan\left(\frac{(p^2 + m_s^2 - m_u^2)}{\mathcal{G}(p^2)}\right)\right] - \frac{1}{p^2}. \tag{A10}$$

APPENDIX B: RQM MODEL PARAMETER FIXING AND THE EFFECTIVE POTENTIAL

The tree-level parameters of Eqs. (37)–(40) become inconsistent after including the quark one-loop vacuum correction unless the on-shell renormalization scheme is used. In the on-shell scheme, one uses the dimensional regularization to regularize the divergent loop integrals, but the counterterms are chosen differently from the minimal subtraction scheme. The appropriate choice of counterterms in the on-shell scheme gives rise to the exact cancellation of the loop corrections with the self-energies. The renormalized parameters become renormalization scale independent as the couplings are evaluated on shell. The wave functions/fields and parameters of Eq. (4) are bare quantities.

The counterterms δZ_π, δZ_K, δZ_σ, δZ_η, $\delta Z_{\eta'}$, δZ_ψ $\delta Z_{\bar\sigma_x}$, and $\delta Z_{\bar\sigma_y}$ for the wave functions/fields and the counterterms δm^2, $\delta\lambda_1$, $\delta\lambda_2$, δc, δh_x, δh_y, and δg^2 for the parameters are introduced in the Lagrangian (4) where the couplings and renormalized fields are defined as

$$\pi_b^i = \sqrt{Z_\pi}\pi^i, \qquad K_b = \sqrt{Z_K}K, \qquad \eta_b = \sqrt{Z_\eta}\eta, \tag{B1}$$

$$\eta'_b = \sqrt{Z_{\eta'}}\eta', \qquad \sigma_b = \sqrt{Z_\sigma}\sigma, \qquad m_b^2 = Z_m m^2, \tag{B2}$$

$$\psi_b = \sqrt{Z_\psi}\psi, \qquad \lambda_{1b} = Z_{\lambda_1}\lambda_1, \qquad \lambda_{2b} = Z_{\lambda_2}\lambda_2, \tag{B3}$$

$$g_b = \sqrt{Z_g}g, \qquad h_{xb} = Z_{h_x}h_x, \qquad h_{yb} = Z_{h_y}h_y, \tag{B4}$$

$$c_b = Z_c c, \qquad \bar\sigma_{xb} = \sqrt{Z_{\bar\sigma_x}}\bar\sigma_x, \qquad \bar\sigma_{y_b} = \sqrt{Z_{\bar\sigma_y}}\bar\sigma_y. \tag{B5}$$

Here, $Z_{(\pi,K,\eta,\eta',\sigma,\psi,\bar\sigma_x,\bar\sigma_y)} = 1 + \delta Z_{(\pi,K,\eta,\eta',\sigma,\psi,\bar\sigma_x,\bar\sigma_y)}$ identifies the field strength renormalization constants while $Z_{(m,\lambda_1,\lambda_2,g,h_x,h_y,c)} = 1 + \delta Z_{(m,\lambda_1,\lambda_2,g,h_x,h_y,c)}$ signifies the mass and coupling renormalization constants.

One-loop corrections to the quark fields and the quark masses are zero because in the large N_c limit the π and σ loops that may renormalize the quark propagators are of the order N_c^0. Hence, $Z_\psi = 1$, and the respective quark self-energy corrections for the nonstrange and the strange quarks are $\delta m_u = 0$ and $\delta m_s = 0$. Since, the pion-quark $\pi\bar\psi\psi$ vertex is of order N_c^0, the one-loop correction gets neglected. As a result, one gets $Z_\psi\sqrt{Z_g g^2}\sqrt{Z_\pi} \approx g(1+\frac{1}{2}\frac{\delta g^2}{g^2} + \frac{1}{2}\delta Z_\pi) = g$. Thus, $\frac{\delta g^2}{g^2} + \delta Z_\pi = 0$;. The $\delta m_u = 0$ and $\delta m_s = 0$ implies that $\delta g\bar\sigma_x/2 + g\delta\bar\sigma_x/2 = 0$ and $\delta g\bar\sigma_y/\sqrt{2} + g\delta\bar\sigma_y/\sqrt{2} = 0$. One gets $\delta\bar\sigma_x/\bar\sigma_x = \delta\bar\sigma_y/\bar\sigma_y = -\delta g/g$ which can be written as

$$\frac{\delta\bar\sigma_x^2}{\bar\sigma_x^2} = \frac{\delta\bar\sigma_y^2}{\bar\sigma_y^2} = -\frac{\delta g^2}{g^2} = \delta Z_\pi. \tag{B6}$$

The fixing of model parameters using the on-shell method requires the expressions of the self-energies of the pseudoscalar pion (π), kaon (K), eta (η), eta-prime (η'), and scalar sigma σ meson. The Feynman diagrams and corresponding expressions for the self-energy corrections, tadpole contributions, and counterterms for the scalar and pseudoscalar particles are given in detail in Ref. [80]. The physical states (masses and self-energies) of the scalar (s) mesons σ, f_0, and the pseudoscalar (p) mesons η, η' are obtained by the corresponding mixing in the 00 and 88 components of the scalar and pseudoscalar particle states (masses and self-energies).

The quark one-loop correction to the one-point function of the nonstrange and strange components of the scalar σ and their tadpole counterterms can be written as

$$\delta\Gamma_x^{(1)} = -4N_c g m_u \mathcal{A}(m_u^2) + i\delta t_x, \tag{B7}$$

$$\delta\Gamma_y^{(1)} = -2\sqrt{2}N_c g m_s \mathcal{A}(m_s^2) + i\delta t_y. \tag{B8}$$

The respective one-point functions $\Gamma_x^{(1)} = it_x = i(h_x - m_\pi^2\bar\sigma_x)$ and $\Gamma_y^{(1)} = it_y = i\{h_y - \frac{\sqrt{2}}{2}(m_K^2 - m_\pi^2)\bar\sigma_x - m_K^2\bar\sigma_y\}$ for the nonstrange and strange degrees of freedom become zero, and one gets two tree-level equations of motion, $t_x = 0$ and $t_y = 0$. Hence, the classical minimum of the effective potential gets fixed. The first renormalization condition for the nonstrange $\langle\bar\sigma_x\rangle = 0$ and the strange degree of freedom $\langle\bar\sigma_y\rangle = 0$ demands that the respective one-loop corrections $\delta\Gamma_x^{(1)}$ and $\delta\Gamma_y^{(1)}$ to the one-point functions become zero, and the minimum of the effective potential does not shift. Putting $\delta\Gamma_x^{(1)} = 0$ and $\delta\Gamma_y^{(1)} = 0$, one gets

$$\delta t_x = -4iN_c g m_u \mathcal{A}(m_u^2), \tag{B9}$$

$$\delta t_y = -2\sqrt{2}iN_c g m_s \mathcal{A}(m_s^2). \tag{B10}$$

The equations $h_x = t_x + m_\pi^2 \bar{\sigma}_x$ and $h_y = t_y + \{\frac{\sqrt{2}}{2}(m_K^2 - m_\pi^2)\bar{\sigma}_x + m_K^2 \bar{\sigma}_y\}$ are used to write the counterterms δh_x and δh_y in terms of the corresponding tadpole counterterms δt_x and δt_y as the following:

$$\delta h_x = m_\pi^2 \delta\bar{\sigma}_x + \delta m_\pi^2 \bar{\sigma}_x + \delta t_x, \tag{B11}$$

$$\delta h_y = \left\{\frac{\sqrt{2}}{2}(m_K^2 - m_\pi^2)\delta\bar{\sigma}_x + \frac{\sqrt{2}}{2}(\delta m_K^2 - \delta m_\pi^2)\bar{\sigma}_x\right\} + m_K^2 \delta\bar{\sigma}_y + \delta m_K^2 \bar{\sigma}_y + \delta t_y. \tag{B12}$$

Using Eq. (B6), one writes

$$\delta h_x = \frac{1}{2} m_\pi^2 \bar{\sigma}_x \delta Z_\pi + \delta m_\pi^2 \bar{\sigma}_x + \delta t_x, \tag{B13}$$

$$\delta h_y = \left\{\frac{\sqrt{2}}{2}(m_K^2 - m_\pi^2)\bar{\sigma}_x \frac{\delta Z_\pi}{2} + \frac{\sqrt{2}}{2}(\delta m_K^2 - \delta m_\pi^2)\bar{\sigma}_x\right\} + m_K^2 \bar{\sigma}_y \frac{\delta Z_\pi}{2} + \delta m_K^2 \bar{\sigma}_y + \delta t_y. \tag{B14}$$

The scalar σ and pseudoscalar η, η', π, and K meson inverse propagators are defined as

$$p^2 - m_{\sigma,\eta,\eta',\pi,K}^2 - i\Sigma_{\sigma,\eta,\eta',\pi,K}(p^2) + \text{counterterms}. \tag{B15}$$

In the Lagrangian, the renormalized mass is made equal to the physical mass, i.e., $m = m_{\text{pole}}$,[1] when one implements the on-shell scheme. One writes

$$\Sigma(p^2 = m_{\sigma,\eta,\eta',\pi,K}^2) + \text{counterterms} = 0. \tag{B16}$$

The propagator residue is set to 1 in the on-shell scheme, and one gets

$$\frac{\partial}{\partial p^2}\Sigma_{\sigma,\eta,\eta',\pi,K}(p^2)\bigg|_{p^2 = m^2_{\sigma,\eta,\eta',\pi,K}} + \text{counterterms} = 0. \tag{B17}$$

Following Ref. [80], the counterterms of the two-point functions of the scalar and pseudoscalar mesons are written below as

$$\Sigma_\sigma^{\text{ct1}}(p^2) = i[\delta Z_\sigma(p^2 - m_\sigma^2) - \delta m_\sigma^2], \tag{B18}$$

$$\Sigma_\pi^{\text{ct1}}(p^2) = i[\delta Z_\pi(p^2 - m_\pi^2) - \delta m_\pi^2], \tag{B19}$$

$$\Sigma_K^{\text{ct1}}(p^2) = i[\delta Z_K(p^2 - m_K^2) - \delta m_K^2], \tag{B20}$$

$$\Sigma_\eta^{\text{ct1}}(p^2) = i[\delta Z_\eta(p^2 - m_\eta^2) - \delta m_\eta^2], \tag{B21}$$

$$\Sigma_{\eta'}^{\text{ct1}}(p^2) = i[\delta Z_{\eta'}(p^2 - m_{\eta'}^2) - \delta m_{\eta'}^2]. \tag{B22}$$

The scalar and pseudoscalar self-energy tadpole contributions have two independent terms proportional to $N_c g m_u \mathcal{A}(m_u^2)$ and $N_c g m_s \mathcal{A}(m_s^2)$, respectively, as given in Appendix B of Ref. [80]. The tadpole counterterms Σ^{ct2} for the scalar and pseudoscalar particles are chosen (negative of the respective tadpole contributions to the scalar and pseudoscalar self-energies) such that they completely cancel the respective tadpole contributions to the self-energies. When the self-energies and their derivatives are evaluated in the on-shell conditions, one gets all the renormalization constants. Combining Eqs. (B16)–(B22), one finds the set of equations given below,

$$\delta m_\pi^2 = -i\Sigma_\pi(m_\pi^2);\ \delta Z_\pi = i\frac{\partial}{\partial p^2}\Sigma_\pi(p^2)\bigg|_{p^2 = m_\pi^2}, \tag{B23}$$

$$\delta m_K^2 = -i\Sigma_K(m_K^2);\ \delta Z_K = i\frac{\partial}{\partial p^2}\Sigma_K(p^2)\bigg|_{p^2 = m_K^2}, \tag{B24}$$

$$\delta m_\eta^2 = -i\Sigma_\eta(m_\eta^2);\ \delta Z_\eta = i\frac{\partial}{\partial p^2}\Sigma_\eta(p^2)\bigg|_{p^2 = m_\eta^2}, \tag{B25}$$

$$\delta m_{\eta'}^2 = -i\Sigma_{\eta'}(m_{\eta'}^2);\ \delta Z_{\eta'} = i\frac{\partial}{\partial p^2}\Sigma_{\eta'}(p^2)\bigg|_{p^2 = m_{\eta'}^2}, \tag{B26}$$

$$\delta m_\sigma^2 = -i\Sigma_\sigma(m_\sigma^2);\ \delta Z_\sigma = i\frac{\partial}{\partial p^2}\Sigma_\sigma(p^2)\bigg|_{p^2 = m_\sigma^2}. \tag{B27}$$

Using the expressions of self-energies for the scalar σ and pseudoscalar η, η', π, and K mesons given in Ref. [80], one gets the following equations:

$$\delta m_\pi^2 = 2ig^2 N_c\left[\mathcal{A}(m_u^2) - \frac{1}{2}m_\pi^2 \mathcal{B}(m_\pi^2, m_u)\right], \tag{B28}$$

$$\delta m_K^2 = ig^2 N_c[\mathcal{A}(m_u^2) + \mathcal{A}(m_s^2) - \{m_K^2 - (m_u - m_s)^2\}\mathcal{B}(m_K^2, m_u, m_s)], \tag{B29}$$

[1]The contributions of the imaginary parts of the self-energies for defining the mass are neglected.

$$\delta m_\eta^2 = \frac{-i}{2}\left[\Sigma_{\mathrm{p},00}(m_\eta^2)+\Sigma_{\mathrm{p},88}(m_\eta^2)-\frac{1}{\sqrt{(m_{\mathrm{p},00}^2-m_{\mathrm{p},88}^2)^2+4m_{\mathrm{p},08}^4}}\right.$$
$$\left.\times\left\{(\Sigma_{\mathrm{p},00}(m_\eta^2)-\Sigma_{\mathrm{p},88}(m_\eta^2))(m_{\mathrm{p},00}^2-m_{\mathrm{p},88}^2)+4\Sigma_{\mathrm{p},08}(m_\eta^2)m_{\mathrm{p},08}^2\right\}\right], \tag{B30}$$

$$\delta m_\eta^2 = ig^2N_c\left[\left\{\mathcal{A}(m_u^2)+\mathcal{A}(m_s^2)-\frac{1}{2}m_\eta^2\mathcal{B}(m_\eta^2,m_u)-\frac{1}{2}m_\eta^2\mathcal{B}(m_\eta^2,m_s)\right\}\right.$$
$$\left.-\frac{\{(m_{\mathrm{p},00}^2-m_{\mathrm{p},88}^2)+4\sqrt{2}m_{\mathrm{p},08}^2\}}{3\sqrt{(m_{\mathrm{p},00}^2-m_{\mathrm{p},88}^2)^2+4m_{\mathrm{p},08}^4}}\left\{\mathcal{A}(m_u^2)-\mathcal{A}(m_s^2)-\frac{1}{2}m_\eta^2\mathcal{B}(m_\eta^2,m_u)+\frac{1}{2}m_\eta^2\mathcal{B}(m_\eta^2,m_s)\right\}\right], \tag{B31}$$

$$\delta m_{\eta'}^2 = \frac{-i}{2}\left[\Sigma_{\mathrm{p},00}(m_{\eta'}^2)+\Sigma_{\mathrm{p},88}(m_{\eta'}^2)+\frac{1}{\sqrt{(m_{\mathrm{p},00}^2-m_{\mathrm{p},88}^2)^2+4m_{\mathrm{p},08}^4}}\right.$$
$$\left.\times\left\{(\Sigma_{\mathrm{p},00}(m_{\eta'}^2)-\Sigma_{\mathrm{p},88}(m_{\eta'}^2))(m_{\mathrm{p},00}^2-m_{\mathrm{p},88}^2)+4\Sigma_{\mathrm{p},08}(m_{\eta'}^2)m_{\mathrm{p},08}^2\right\}\right], \tag{B32}$$

$$\delta m_{\eta'}^2 = ig^2N_c\left[\left\{\mathcal{A}(m_u^2)+\mathcal{A}(m_s^2)-\frac{1}{2}m_{\eta'}^2\mathcal{B}(m_{\eta'}^2,m_u)-\frac{1}{2}m_{\eta'}^2\mathcal{B}(m_{\eta'}^2,m_s)\right\}\right.$$
$$\left.+\frac{\{(m_{\mathrm{p},00}^2-m_{\mathrm{p},88}^2)+4\sqrt{2}m_{\mathrm{p},08}^2\}}{3\sqrt{(m_{\mathrm{p},00}^2-m_{\mathrm{p},88}^2)^2+4m_{\mathrm{p},08}^4}}\left\{\mathcal{A}(m_u^2)-\mathcal{A}(m_s^2)-\frac{1}{2}m_{\eta'}^2\mathcal{B}(m_{\eta'}^2,m_u)+\frac{1}{2}m_{\eta'}^2\mathcal{B}(m_{\eta'}^2,m_s)\right\}\right], \tag{B33}$$

$$\delta m_\sigma^2 = \frac{-i}{2}\left[\Sigma_{\mathrm{s},00}(m_\sigma^2)+\Sigma_{\mathrm{s},88}(m_\sigma^2)-\frac{1}{\sqrt{(m_{\mathrm{s},00}^2-m_{\mathrm{s},88}^2)^2+4m_{\mathrm{s},08}^4}}\right.$$
$$\left.\times\left\{(\Sigma_{\mathrm{s},00}(m_\sigma^2)-\Sigma_{\mathrm{s},88}(m_\sigma^2))(m_{\mathrm{s},00}^2-m_{\mathrm{s},88}^2)+4\Sigma_{\mathrm{s},08}(m_\sigma^2)m_{\mathrm{s},08}^2\right\}\right], \tag{B34}$$

$$\delta m_\sigma^2 = ig^2N_c\left[\left\{\mathcal{A}(m_u^2)+\mathcal{A}(m_s^2)-\frac{1}{2}(m_\sigma^2-4m_u^2)\mathcal{B}(m_\sigma^2,m_u)-\frac{1}{2}(m_\sigma^2-4m_s^2)\mathcal{B}(m_\sigma^2,m_s)\right\}\right.$$
$$\left.-\frac{\{(m_{\mathrm{s},00}^2-m_{\mathrm{s},88}^2)+4\sqrt{2}m_{\mathrm{s},08}^2\}}{3\sqrt{(m_{\mathrm{s},00}^2-m_{\mathrm{s},88}^2)^2+4m_{\mathrm{s},08}^4}}\left\{\mathcal{A}(m_u^2)-\mathcal{A}(m_s^2)-\frac{(m_\sigma^2-4m_u^2)}{2}\mathcal{B}(m_\sigma^2,m_u)+\frac{(m_\sigma^2-4m_s^2)}{2}\mathcal{B}(m_\sigma^2,m_s)\right\}\right], \tag{B35}$$

$$\delta Z_\pi = ig^2N_c[\mathcal{B}(m_\pi^2,m_u)+m_\pi^2\mathcal{B}'(m_\pi^2,m_u)], \tag{B36}$$

$$\delta Z_K = ig^2N_c[\mathcal{B}(m_K^2,m_u,m_s)+(m_K^2-(m_u-m_s)^2)\mathcal{B}'(m_K^2,m_u,m_s)], \tag{B37}$$

$$\delta Z_\eta = \frac{ig^2N_c}{2}\left[\{\mathcal{B}(m_\eta^2,m_u)+\mathcal{B}(m_\eta^2,m_s)+m_\eta^2\mathcal{B}'(m_\eta^2,m_u)+m_\eta^2\mathcal{B}'(m_\eta^2,m_s)\}\right.$$
$$\left.+\frac{\{(m_{\mathrm{p},00}^2-m_{\mathrm{p},88}^2)+4\sqrt{2}m_{\mathrm{p},08}^2\}}{3\sqrt{(m_{\mathrm{p},00}^2-m_{\mathrm{p},88}^2)^2+4m_{\mathrm{p},08}^4}}\{-\mathcal{B}(m_\eta^2,m_u)+\mathcal{B}(m_\eta^2,m_s)-m_\eta^2\mathcal{B}'(m_\eta^2,m_u)+m_\eta^2\mathcal{B}'(m_\eta^2,m_s)\}\right], \tag{B38}$$

$$\delta Z_{\eta'} = \frac{ig^2N_c}{2}\left[\{\mathcal{B}(m_{\eta'}^2,m_u)+\mathcal{B}(m_{\eta'}^2,m_s)+m_{\eta'}^2\mathcal{B}'(m_{\eta'}^2,m_u)+m_{\eta'}^2\mathcal{B}'(m_{\eta'}^2,m_s)\}\right.$$
$$\left.-\frac{\{(m_{\mathrm{p},00}^2-m_{\mathrm{p},88}^2)+4\sqrt{2}m_{\mathrm{p},08}^2\}}{3\sqrt{(m_{\mathrm{p},00}^2-m_{\mathrm{p},88}^2)^2+4m_{\mathrm{p},08}^4}}\{-\mathcal{B}(m_{\eta'}^2,m_u)+\mathcal{B}(m_{\eta'}^2,m_s)-m_{\eta'}^2\mathcal{B}'(m_{\eta'}^2,m_u)+m_{\eta'}^2\mathcal{B}'(m_{\eta'}^2,m_s)\}\right], \tag{B39}$$

$$\delta Z_\sigma = \frac{ig^2 N_c}{2}\Bigg[\{\mathcal{B}(m_\sigma^2, m_u) + \mathcal{B}(m_\sigma^2, m_s) + (m_\sigma^2 - 4m_u^2)\mathcal{B}'(m_\sigma^2, m_u) + (m_\sigma^2 - 4m_s^2)\mathcal{B}'(m_\sigma^2, m_s)\} + \frac{\{(m_{s,00}^2 - m_{s,88}^2) + 4\sqrt{2}m_{s,08}^2\}}{3\sqrt{(m_{s,00}^2 - m_{s,88}^2)^2 + 4m_{s,08}^4}}\Big\{\mathcal{B}(m_\sigma^2, m_s) - \mathcal{B}(m_\sigma^2, m_u) - (m_\sigma^2 - 4m_u^2)\mathcal{B}'(m_\sigma^2, m_u) + (m_\sigma^2 - 4m_s^2)\mathcal{B}'(m_\sigma^2, m_s)\Big\}\Bigg]. \tag{B40}$$

The expressions of the field renormalization constants for π, K, η, η', and σ are given above. However, one needs to have the simplified expression of δZ_π only in the calculations below.

Following Refs. [70,76–80,95] and using Eqs. (B1)–(B5) together with Eqs. (37) and (38), $\delta\lambda_2$ can be expressed in terms of the above given expressions of δm_π^2, δm_K^2, δm_η^2, $\delta m_{\eta'}^2$, and δZ_π. The δc can be expressed in terms of the expressions of δm_π^2, δm_K^2, δZ_π and the preceding $\delta\lambda_2$. The $\delta\lambda_2$ is written as the following:

$$\delta\lambda_2 = -\lambda_2\delta Z_\pi + \frac{2}{(\bar\sigma_x^2 + 4\bar\sigma_y^2)(\sqrt{2}\bar\sigma_y - \bar\sigma_x)}\Big[(3\sqrt{2}\bar\sigma_y)\delta m_K^2 - (\sqrt{2}\bar\sigma_y + 2\bar\sigma_x)\delta m_\pi^2 - (\sqrt{2}\bar\sigma_y - \bar\sigma_x)(\delta m_\eta^2 + \delta m_{\eta'}^2)\Big]. \tag{B41}$$

The δc is written below as

$$\delta c = \frac{2(\delta m_K^2 - \delta m_\pi^2)}{(\sqrt{2}\bar\sigma_y - \bar\sigma_x)} - \sqrt{2}\bar\sigma_y\delta\lambda_2 - (2\sqrt{2}\bar\sigma_y\lambda_2 + c)\frac{\delta Z_\pi}{2}. \tag{B42}$$

Knowing $\delta\lambda_2$ and δc and using the expression of $(\delta m_\sigma^2 - \delta m_\pi^2)$, $\delta\lambda_1$ can be written after some algebraic manipulations as the following:

$$\delta\lambda_1 = \frac{\delta\lambda_{1\mathrm{NUMI}}}{\lambda_{1\mathrm{DENOM}}} - \lambda_1\delta Z_\pi, \tag{B43}$$

$$\lambda_{1\mathrm{DENOM}} = \left(\sqrt{(m_{s,00}^2 - m_{s,88}^2)^2 + 4m_{s,08}^4}\right)(\bar\sigma_x^2 + \bar\sigma_y^2) - \frac{(m_{s,00}^2 - m_{s,88}^2)}{3}(\bar\sigma_x^2 + 4\sqrt{2}\bar\sigma_x\bar\sigma_y - \bar\sigma_y^2) - \frac{4m_{s,08}^2}{3}(\sqrt{2}\bar\sigma_x^2 - \bar\sigma_x\bar\sigma_y - \sqrt{2}\bar\sigma_y^2), \tag{B44}$$

$$\begin{aligned}\delta\lambda_{1\mathrm{NUMI}} = {} & \sqrt{(m_{s,00}^2 - m_{s,88}^2)^2 + 4m_{s,08}^4}(\delta m_\sigma^2 - \delta m_\pi^2) - \left\{\delta\lambda_2\frac{(\bar\sigma_x^2 + 6\bar\sigma_y^2)}{4} + \delta c\frac{\sqrt{2}\bar\sigma_y}{4}\right\}\sqrt{(m_{s,00}^2 - m_{s,88}^2)^2 + 4m_{s,08}^4} \\ & + \left\{\delta\lambda_2\frac{(\bar\sigma_x^2 - 2\bar\sigma_y^2)}{4} - \delta c\frac{\sqrt{2}(4\sqrt{2}\bar\sigma_x + \bar\sigma_y)}{12}\right\}(m_{s,00}^2 - m_{s,88}^2) + \left\{\delta\lambda_2\sqrt{2}(\bar\sigma_x^2 - 2\bar\sigma_y^2) + \delta c\frac{\sqrt{2}(\bar\sigma_x - \sqrt{2}\bar\sigma_y)}{3}\right\}m_{s,08}^2 \\ & - \lambda_2\delta Z_\pi\left\{\frac{(\bar\sigma_x^2 + 6\bar\sigma_y^2)}{4}\sqrt{(m_{s,00}^2 - m_{s,88}^2)^2 + 4m_{s,08}^4} - \frac{(\bar\sigma_x^2 - 2\bar\sigma_y^2)}{4}(m_{s,00}^2 - m_{s,88}^2) - \sqrt{2}(\bar\sigma_x^2 - 2\bar\sigma_y^2)m_{s,08}^2\right\} \\ & - c\frac{\delta Z_\pi}{2}\left\{\frac{\sqrt{2}\bar\sigma_y}{4}\sqrt{(m_{s,00}^2 - m_{s,88}^2)^2 + 4m_{s,08}^4} + \frac{\sqrt{2}(4\sqrt{2}\bar\sigma_x + \bar\sigma_y)}{12}(m_{s,00}^2 - m_{s,88}^2) + \frac{\sqrt{2}(\sqrt{2}\bar\sigma_y - \bar\sigma_x)}{3}m_{s,08}^2\right\}.\end{aligned} \tag{B45}$$

The counterterm δm^2 is written in terms of $\delta m_\pi^2, \delta\lambda_1, \delta\lambda_2, \delta c$ and δZ_π as

$$\delta m^2 = \delta m_\pi^2 - \delta\lambda_1(\bar\sigma_x^2 + \bar\sigma_y^2) - \frac{(\delta\lambda_2)\bar\sigma_x^2}{2} + \frac{\delta c\bar\sigma_y}{\sqrt{2}} - \delta Z_\pi\left\{\lambda_1(\bar\sigma_x^2 + \bar\sigma_y^2) + \frac{\lambda_2\bar\sigma_x^2}{2} - \frac{c\bar\sigma_y}{2\sqrt{2}}\right\}. \tag{B46}$$

When we substitute the expressions of $\delta Z_\pi, \delta m_K^2, \delta m_\pi^2, \delta m_\eta^2$, and $\delta m_{\eta'}^2$ from the above in Eq. (B41), we get the expression of $\delta\lambda_2$ as written below,

$$\delta\lambda_{2\mathrm{OS}} = \frac{2iN_c g^2}{(\bar{\sigma}_x^2+4\bar{\sigma}_y^2)(\sqrt{2}\bar{\sigma}_y-\bar{\sigma}_x)}\Bigg[(3\sqrt{2}\bar{\sigma}_y)\{\mathcal{A}(m_u^2)+\mathcal{A}(m_s^2)-(m_K^2-(m_s-m_u)^2)\mathcal{B}(m_K^2,m_u,m_s)\}$$
$$-(\sqrt{2}\bar{\sigma}_y+2\bar{\sigma}_x)\{2\mathcal{A}(m_u^2)-m_\pi^2\mathcal{B}(m_\pi^2,m_u)\}-(\sqrt{2}\bar{\sigma}_y-\bar{\sigma}_x)\Bigg\{2\mathcal{A}(m_u^2)+2\mathcal{A}(m_s^2)-\frac{m_\eta^2}{2}\{\mathcal{B}(m_\eta^2,m_u)$$
$$+\mathcal{B}(m_\eta^2,m_s)\}-\frac{m_{\eta'}^2}{2}\{\mathcal{B}(m_{\eta'}^2,m_u)+\mathcal{B}(m_{\eta'}^2,m_s)\}-\frac{(m_{p,00}^2-m_{p,88}^2+4\sqrt{2}m_{p,08}^2)}{6\left(\sqrt{(m_{p,00}^2-m_{p,88}^2)^2+4m_{p,08}^4}\right)}$$
$$\times\{m_\eta^2\{-\mathcal{B}(m_\eta^2,m_u)+\mathcal{B}(m_\eta^2,m_s)\}-m_{\eta'}^2\{-\mathcal{B}(m_{\eta'}^2,m_u)+\mathcal{B}(m_{\eta'}^2,m_s)\}\}\Bigg\}\Bigg]. \tag{B47}$$

Here, a common factor SCF is defined below as

$$\mathrm{SCF}=\left[\ln\left(\frac{\Lambda^2}{m_u^2}\right)+\mathcal{C}(m_\pi^2,m_u)+m_\pi^2\mathcal{C}'(m_\pi^2,m_u)\right], \tag{B48}$$

$$\delta\lambda_{2\mathrm{OS}}=\delta\lambda_{2\mathrm{div}}+\lambda_{2\mathrm{FIN}}+\lambda_{2\mathrm{SCF}},\qquad \lambda_{2\mathrm{SCF}}=\frac{N_c g^2\lambda_2}{(4\pi)^2}\mathrm{SCF}, \tag{B49}$$

$$\lambda_{2\mathrm{FIN}}=\frac{N_c g^2}{(4\pi)^2}(\lambda_2-g^2)\ln\left(\frac{\Lambda^2}{m_u^2}\right)+\frac{N_c g^2}{(4\pi)^2}\frac{2}{(\bar{\sigma}_x^2+4\bar{\sigma}_y^2)}\Bigg[\frac{(\sqrt{2}\bar{\sigma}_y+2\bar{\sigma}_x)}{(\sqrt{2}\bar{\sigma}_y-\bar{\sigma}_x)}\Bigg\{m_u^2-m_s^2\Bigg\{1-2\ln\left(\frac{m_s}{m_u}\right)\Bigg\}$$
$$-m_\pi^2\mathcal{C}(m_\pi^2,m_u)\Bigg\}+\frac{3\sqrt{2}\bar{\sigma}_y}{(\sqrt{2}\bar{\sigma}_y-\bar{\sigma}_x)}\{m_K^2-(m_s-m_u)^2\}\mathcal{C}(m_K^2,m_u,m_s)-\frac{m_\eta^2}{2}\Bigg\{\mathcal{C}(m_\eta^2,m_u)+\mathcal{C}(m_\eta^2,m_s)$$
$$-2\ln\left(\frac{m_s}{m_u}\right)\Bigg\}-\frac{m_{\eta'}^2}{2}\Bigg\{\mathcal{C}(m_{\eta'}^2,m_u)+\mathcal{C}(m_{\eta'}^2,m_s)-2\ln\left(\frac{m_s}{m_u}\right)\Bigg\}+\frac{(m_{p,00}^2-m_{p,88}^2+4\sqrt{2}m_{p,08}^2)}{6(\sqrt{(m_{p,00}^2-m_{p,88}^2)^2+4m_{p,08}^4})}$$
$$\times\Bigg\{m_\eta^2\Bigg\{\mathcal{C}(m_\eta^2,m_u)-\mathcal{C}(m_\eta^2,m_s)+2\ln\left(\frac{m_s}{m_u}\right)\Bigg\}-m_{\eta'}^2\Bigg\{\mathcal{C}(m_{\eta'}^2,m_u)-\mathcal{C}(m_{\eta'}^2,m_s)+2\ln\left(\frac{m_s}{m_u}\right)\Bigg\}\Bigg\}\Bigg]. \tag{B50}$$

Substituting the expressions of $\delta Z_\pi, \delta m_K^2, \delta m_\pi^2, \delta\lambda_2$ in Eq. (42), δc is written as

$$\delta c_{\mathrm{OS}}=\frac{2iN_c g^2}{(\sqrt{2}\bar{\sigma}_y-\bar{\sigma}_x)}\{\mathcal{A}(m_u^2)+\mathcal{A}(m_s^2)-(m_K^2-(m_s-m_u)^2)\mathcal{B}(m_K^2,m_u,m_s)-2\mathcal{A}(m_u^2)+m_\pi^2\mathcal{B}(m_\pi^2,m_u)\}$$
$$-\sqrt{2}\bar{\sigma}_y\delta\lambda_{2\mathrm{OS}}-(2\sqrt{2}\bar{\sigma}_y\lambda_2+c)\frac{\delta Z_\pi}{2}, \tag{B51}$$

$$\delta c_{\mathrm{OS}}=\delta c_{\mathrm{div}}+c_{\mathrm{FINTOT}}+c_{\mathrm{SCF}},\qquad c_{\mathrm{FINTOT}}=-\sqrt{2}\bar{\sigma}_y\lambda_{2\mathrm{FIN}}+c_{\mathrm{FIN}}, \tag{B52}$$

$$c_{\mathrm{FIN}}=\frac{N_c g^2}{(4\pi)^2}\Bigg[\{c+\sqrt{2}\bar{\sigma}_y(\lambda_2-g^2)\}\ln\left(\frac{\Lambda^2}{m_u^2}\right)+\frac{2}{(\sqrt{2}\bar{\sigma}_y-\bar{\sigma}_x)}\{\{m_K^2-(m_s-m_u)^2\}\mathcal{C}(m_K^2,m_u,m_s)-m_\pi^2\mathcal{C}(m_\pi^2,m_u)\}$$
$$-\frac{g^2}{2}(\sqrt{2}\bar{\sigma}_y+\bar{\sigma}_x)+\frac{2g^2\bar{\sigma}_y^2}{(\sqrt{2}\bar{\sigma}_y-\bar{\sigma}_x)}\ln\left(\frac{m_s}{m_u}\right)\Bigg],\qquad c_{\mathrm{SCF}}=\frac{N_c g^2 c}{2(4\pi)^2}\mathrm{SCF}. \tag{B53}$$

Using Eq. (B43) and substituting the expressions of $\delta Z_\pi, \delta m_\sigma^2, \delta m_\pi^2, \delta\lambda_2$, and δc in Eq. (B45), $\delta\lambda_1$ is written as

$$\delta\lambda_{1\mathrm{OS}}=\frac{\lambda_{1\mathrm{NUMOS}}}{\lambda_{1\mathrm{DENOM}}}-\lambda_1\delta Z_\pi, \tag{B54}$$

$$\lambda_{1\mathrm{NUMOS}} = iN_c g^2 \Bigg[\left(\sqrt{(m_{s,00}^2 - m_{s,88}^2)^2 + 4m_{s,08}^4} \right) \Bigg\{ \mathcal{A}(m_u^2) + \mathcal{A}(m_s^2) - \left(\frac{m_\sigma^2 - 4m_u^2}{2} \right) \mathcal{B}(m_\sigma^2, m_u) - \left(\frac{m_\sigma^2 - 4m_s^2}{2} \right) \times \mathcal{B}(m_\sigma^2, m_s) - 2\mathcal{A}(m_u^2) + m_\pi^2 \mathcal{B}(m_\pi^2, m_u) \Bigg\} - \left(\frac{m_{s,00}^2 - m_{s,88}^2 + 4\sqrt{2} m_{s,08}^2}{3} \right) \Bigg\{ \mathcal{A}(m_u^2) - \mathcal{A}(m_s^2) - \left(\frac{m_\sigma^2 - 4m_u^2}{2} \right) \times \mathcal{B}(m_\sigma^2, m_u) + \left(\frac{m_\sigma^2 - 4m_s^2}{2} \right) \mathcal{B}(m_\sigma^2, m_s) \Bigg\} \Bigg] + \frac{(m_{s,00}^2 - m_{s,88}^2)}{12} \{ (3\bar{\sigma}_x^2 - 6\bar{\sigma}_y^2) \delta\lambda_{2\mathrm{OS}} - \sqrt{2}(4\sqrt{2}\bar{\sigma}_x + \bar{\sigma}_y) \delta c_{\mathrm{OS}} \} - \frac{\sqrt{2} m_{s,08}^2}{3} \{ (2\bar{\sigma}_y^2 - \bar{\sigma}_x^2) \delta\lambda_{2\mathrm{OS}} + (\sqrt{2}\bar{\sigma}_y - \bar{\sigma}_x) \delta c_{\mathrm{OS}} \} - \frac{1}{4} \sqrt{(m_{s,00}^2 - m_{s,88}^2)^2 + 4m_{s,08}^4} \{ (\bar{\sigma}_x^2 + 6\bar{\sigma}_y^2) \delta\lambda_{2\mathrm{OS}} + \sqrt{2}\bar{\sigma}_y \delta c_{\mathrm{OS}} \} + \delta Z_\pi \Bigg[\frac{(m_{\sigma_{00}}^2 - m_{s,88}^2)}{12} \left\{ (3\bar{\sigma}_x^2 - 6\bar{\sigma}_y^2)\lambda_2 - \sqrt{2}(4\sqrt{2}\bar{\sigma}_x + \bar{\sigma}_y) \frac{c}{2} \right\} - \frac{\sqrt{2} m_{s,08}^2}{3} \left\{ (2\bar{\sigma}_y^2 - \bar{\sigma}_x^2)\lambda_2 + (\sqrt{2}\bar{\sigma}_y - \bar{\sigma}_x) \frac{c}{2} \right\} - \frac{1}{4} \left(\sqrt{(m_{s,00}^2 - m_{s,88}^2)^2 + 4m_{s,08}^4} \right) \left\{ (\bar{\sigma}_x^2 + 6\bar{\sigma}_y^2)\lambda_2 + \sqrt{2}\bar{\sigma}_y \frac{c}{2} \right\} \Bigg], \tag{B55}$$

$$\delta\lambda_{1\mathrm{OS}} = \delta\lambda_{1\mathrm{div}} + \lambda_{1\mathrm{FIN}} + \lambda_{1\mathrm{SCF}}, \qquad \lambda_{1\mathrm{SCF}} = \frac{N_c g^2 \lambda_1}{(4\pi)^2} \mathrm{SCF}, \qquad \lambda_{1\mathrm{FIN}} = \frac{\lambda_{1\mathrm{NUMF}}}{\lambda_{1\mathrm{DENOM}}}, \qquad \lambda_{1\mathrm{NUMF}} = \lambda_{1\mathrm{NUMF-I}} + \lambda_{1\mathrm{NUMF-II}}. \tag{B56}$$

The expression of $\lambda_{1\mathrm{DENOM}}$ is given in Eq. (B44),

$$\lambda_{1\mathrm{NUMF-I}} = \frac{(m_{s,00}^2 - m_{s,88}^2)}{12} \left\{ (3\bar{\sigma}_x^2 + 8\sqrt{2}\bar{\sigma}_x\bar{\sigma}_y - 4\bar{\sigma}_y^2)\lambda_{2\mathrm{FIN}} - \sqrt{2}(4\sqrt{2}\bar{\sigma}_x + \bar{\sigma}_y) c_{\mathrm{FIN}} \right\} - \frac{\sqrt{2} m_{s,08}^2}{3} \left\{ (\sqrt{2}\bar{\sigma}_y - \bar{\sigma}_x) c_{\mathrm{FIN}} + (4\bar{\sigma}_y^2 + \sqrt{2}\bar{\sigma}_x\bar{\sigma}_y - 3\bar{\sigma}_x^2)\lambda_{2\mathrm{FIN}} \right\} - \left(\frac{1}{4} \sqrt{(m_{s,00}^2 - m_{s,88}^2)^2 + 4m_{s,08}^4} \right) \left\{ (\bar{\sigma}_x^2 + 4\bar{\sigma}_y^2)\lambda_{2\mathrm{FIN}} + \sqrt{2}\bar{\sigma}_y c_{\mathrm{FIN}} \right\}, \tag{B57}$$

$$\lambda_{1\mathrm{NUMF-II}} = \frac{N_c g^2}{(4\pi)^2} \Bigg[\left(\sqrt{(m_{s,00}^2 - m_{s,88}^2)^2 + 4m_{s,08}^4} \right) \Bigg\{ \frac{g^2}{4} (\bar{\sigma}_x^2 - 2\bar{\sigma}_y^2) + (m_\sigma^2 - m_\pi^2 - m_u^2 - 3m_s^2) \ln\left(\frac{\Lambda^2}{m_u^2} \right) + 2m_s^2 \ln\left(\frac{m_s}{m_u} \right) + \frac{(m_\sigma^2 - 4m_u^2)}{2} \mathcal{C}(m_\sigma^2, m_u) + \frac{(m_\sigma^2 - 4m_s^2)}{2} \left(\mathcal{C}(m_\sigma^2, m_s) - 2\ln\left(\frac{m_s}{m_u} \right) \right) - m_\pi^2 \mathcal{C}(m_\pi^2, m_u) \Bigg\} - \left(\frac{(m_{s,00}^2 - m_{s,88}^2) + 4\sqrt{2} m_{s,08}^2}{3} \right) \Bigg\{ \frac{g^2}{4} (2\bar{\sigma}_y^2 - \bar{\sigma}_x^2) \left(1 + 3\ln\left(\frac{\Lambda^2}{m_u^2} \right) \right) + (m_\sigma^2 - 6m_s^2) \ln\left(\frac{m_s}{m_u} \right) + \frac{(m_\sigma^2 - 4m_u^2)}{2} \mathcal{C}(m_\sigma^2, m_u) - \frac{(m_\sigma^2 - 4m_s^2)}{2} \mathcal{C}(m_\sigma^2, m_s) \Bigg\} \Bigg]. \tag{B58}$$

Using Eq. (B46), δm^2 is written as

$$\delta m_{\mathrm{OS}}^2 = iN_c g^2 \{ 2\mathcal{A}(m_u^2) - m_\pi^2 \mathcal{B}(m_\pi^2, m_u) \} - \delta\lambda_{1\mathrm{OS}} (\bar{\sigma}_x^2 + \bar{\sigma}_y^2) - \delta\lambda_{2\mathrm{OS}} \frac{\bar{\sigma}_x^2}{2} + \frac{\delta c_{\mathrm{OS}} \bar{\sigma}_y}{\sqrt{2}} - \delta Z_\pi \left\{ \lambda_1 (\bar{\sigma}_x^2 + \bar{\sigma}_y^2) + \lambda_2 \frac{\bar{\sigma}_x^2}{2} - \frac{c\bar{\sigma}_y}{2\sqrt{2}} \right\},$$
$$\delta m_{\mathrm{OS}}^2 = \delta m_{\mathrm{div}}^2 + m_{\mathrm{FIN}}^2, \tag{B59}$$

$$m_{\mathrm{FIN}}^2 = \frac{N_c g^2}{(4\pi)^2} \left[-2m_u^2 + (m_\pi^2 - 2m_u^2) \ln\left(\frac{\Lambda^2}{m_u^2} \right) + m_\pi^2 \mathcal{C}(m_\pi^2, m_u) \right] - \left[\lambda_{1\mathrm{FIN}} (\bar{\sigma}_x^2 + \bar{\sigma}_y^2) + \lambda_{2\mathrm{FIN}} \frac{\bar{\sigma}_x^2}{2} - c_{\mathrm{FINTOT}} \frac{\bar{\sigma}_y}{\sqrt{2}} \right]. \tag{B60}$$

Using Eqs. (B13) and (B14), δh_x and δh_y is written as

$$\delta h_{x\mathrm{OS}} = -\frac{i}{2} N_c g^2 m_\pi^2 \bar{\sigma}_x [\mathcal{B}(m_\pi^2, m_u) - m_\pi^2 \mathcal{B}'(m_\pi^2, m_u)], \tag{B61}$$

$$\delta h_{x\mathrm{OS}} = \delta h_{x\mathrm{div}} + h_{x\mathrm{FIN}}, \tag{B62}$$

$$h_{x\mathrm{FIN}} = \frac{N_c g^2}{2(4\pi)^2} h_x \left[\ln\left(\frac{\Lambda^2}{m_u^2}\right) + \mathcal{C}(m_\pi^2, m_u) - m_\pi^2 \mathcal{C}'(m_\pi^2, m_u) \right]. \tag{B63}$$

$$\begin{aligned}\delta h_{y\mathrm{OS}} = iN_c g^2 \Bigg[& \left(\frac{\sqrt{2}}{2}\bar{\sigma}_x - \bar{\sigma}_y\right)\{\mathcal{A}(m_s^2) - \mathcal{A}(m_u^2)\} - \left(\frac{\sqrt{2}}{2}\bar{\sigma}_x + \bar{\sigma}_y\right)\{m_K^2 - (m_u - m_s)^2\}\mathcal{B}(m_K^2, m_u, m_s) \\ & + \left(\frac{\sqrt{2}}{2}\bar{\sigma}_x + \bar{\sigma}_y\right)\frac{m_K^2}{2}[\mathcal{B}(m_\pi^2, m_u) + m_\pi^2 \mathcal{B}'(m_\pi^2, m_u)] + \frac{\sqrt{2}}{4}\bar{\sigma}_x m_\pi^2 [\mathcal{B}(m_\pi^2, m_u) - m_\pi^2 \mathcal{B}'(m_\pi^2, m_u)] \Bigg],\end{aligned} \tag{B64}$$

$$\delta h_{y\mathrm{OS}} = \delta h_{y\mathrm{div}} + h_{y\mathrm{FIN}}, \tag{B65}$$

$$\begin{aligned}h_{y\mathrm{FIN}} = \frac{N_c g^2}{(4\pi)^2} \Bigg[& \frac{h_y}{2}\left\{ \ln\left(\frac{\Lambda^2}{m_u^2}\right) - \mathcal{C}(m_\pi^2, m_u) - m_\pi^2 \mathcal{C}'(m_\pi^2, m_u) \right\} - \frac{\sqrt{2}h_x}{2}\mathcal{C}(m_\pi^2, m_u) \\ & + \left(\frac{\sqrt{2}\bar{\sigma}_x}{2} - \bar{\sigma}_y\right)\left\{ m_u^2 - m_s^2 + 2m_s^2 \ln\left(\frac{m_s}{m_u}\right)\right\} + \left(\frac{\sqrt{2}\bar{\sigma}_x}{2} + \bar{\sigma}_y\right)\{m_K^2 - (m_s - m_u)^2\}\mathcal{C}(m_K^2, m_u, m_s) \Bigg].\end{aligned} \tag{B66}$$

Using Eqs. (B6) and (B36), $\delta Z_\pi, \delta g^2, \delta \bar{\sigma}_x{}^2$, and $\delta \bar{\sigma}_y{}^2$ can be written as

$$\delta Z_\pi^{\mathrm{OS}} = \delta Z_{\pi,\mathrm{div}} - \frac{N_c g^2}{(4\pi)^2}\left[\ln\left(\frac{\Lambda^2}{m_u^2}\right) + \mathcal{C}(m_\pi^2, m_u) + m_\pi^2 \mathcal{C}'(m_\pi^2, m_u) \right], \tag{B67}$$

$$\delta g^2_{\mathrm{OS}} = -iN_c g^4 [m_\pi^2 \mathcal{B}'(m_\pi^2, m_u) + \mathcal{B}(m_\pi^2, m_u)] = \delta g^2_{\mathrm{div}} + \frac{N_c g^4}{(4\pi)^2}\left[\ln\left(\frac{\Lambda^2}{m_u^2}\right) + \mathcal{C}(m_\pi^2, m_u) + m_\pi^2 \mathcal{C}'(m_\pi^2, m_u) \right], \tag{B68}$$

$$\delta \bar{\sigma}_x{}^2_{\mathrm{OS}} = iN_c g^2 \bar{\sigma}_x^2 [m_\pi^2 \mathcal{B}'(m_\pi^2, m_u) + \mathcal{B}(m_\pi^2, m_u)] = \delta \bar{\sigma}_x{}^2_{\mathrm{div}} - \frac{N_c g^2 \bar{\sigma}_x^2}{(4\pi)^2}\left[\ln\left(\frac{\Lambda^2}{m_u^2}\right) + \mathcal{C}(m_\pi^2, m_u) + m_\pi^2 \mathcal{C}'(m_\pi^2, m_u) \right], \tag{B69}$$

$$\delta \bar{\sigma}_y{}^2_{\mathrm{OS}} = iN_c g^2 \bar{\sigma}_y^2 [m_\pi^2 \mathcal{B}'(m_\pi^2, m_u) + \mathcal{B}(m_\pi^2, m_u)] = \delta \bar{\sigma}_y{}^2_{\mathrm{div}} - \frac{N_c g^2 \bar{\sigma}_y{}^2}{(4\pi)^2}\left[\ln\left(\frac{\Lambda^2}{m_u^2}\right) + \mathcal{C}(m_\pi^2, m_u) + m_\pi^2 \mathcal{C}'(m_\pi^2, m_u) \right]. \tag{B70}$$

The $\mathcal{A}(m_f^2), \mathcal{B}(m^2, m_f), \mathcal{B}(m^2, m_u, m_s), \mathcal{B}'(m^2, m_f)$, $\mathcal{C}(m^2, m_f)$, $\mathcal{C}(m^2, m_u, m_s)$, $\mathcal{C}'(m^2, m_f)$, and $\mathcal{C}'(m^2, m_u, m_s)$ are defined in Appendix A. The divergent part of the counterterms are $\delta\lambda_{2\mathrm{div}} = \frac{N_c g^2}{(4\pi)^2\epsilon}(2\lambda_2 - g^2)$, $\delta c_{\mathrm{div}} = \frac{3N_c g^2 c}{2(4\pi)^2\epsilon}$, $\delta\lambda_{1\mathrm{div}} = \frac{2N_c g^2 \lambda_1}{(4\pi)^2\epsilon}$, $\delta m^2_{\mathrm{div}} = \frac{N_c g^2 m^2}{(4\pi)^2\epsilon}$, $\delta h_{x\mathrm{div}} = \frac{N_c g^2 h_x}{2(4\pi)^2\epsilon}$, $\delta h_{y\mathrm{div}} = \frac{N_c g^2 h_y}{2(4\pi)^2\epsilon}$, $\delta g^2_{\mathrm{div}} = \frac{N_c g^4}{(4\pi)^2\epsilon}$, $\delta \bar{\sigma}_x{}^2_{\mathrm{div}} = -\frac{N_c g^2 \bar{\sigma}_x^2}{(4\pi)^2\epsilon}$, $\delta \bar{\sigma}_y{}^2_{\mathrm{div}} = -\frac{N_c g^2 \bar{\sigma}_y^2}{(4\pi)^2\epsilon}$, $\delta Z_{\pi,\mathrm{div}} = -\frac{N_c g^2}{(4\pi)^2\epsilon}$. For both the on-shell and the $\overline{\mathrm{MS}}$ schemes, the divergent part of the counterterms are the same, i.e., $\delta\lambda_{1\mathrm{div}} = \delta\lambda_{1\overline{\mathrm{MS}}}$, $\delta\lambda_{2\mathrm{div}} = \delta\lambda_{2\overline{\mathrm{MS}}}$, etc.

Due to the renormalization scheme independence of the bare parameters, one can write down the relations between the renormalized parameters in the on-shell and the $\overline{\mathrm{MS}}$ schemes as given below,

$$\lambda_{2\overline{\mathrm{MS}}} = \lambda_2 + \delta\lambda_{2\mathrm{OS}} - \delta\lambda_{2\overline{\mathrm{MS}}}, \tag{B71}$$

$$c_{\overline{\mathrm{MS}}} = c + \delta c_{\mathrm{OS}} - \delta c_{\overline{\mathrm{MS}}}, \tag{B72}$$

$$\lambda_{1\overline{\mathrm{MS}}} = \lambda_1 + \delta\lambda_{1\mathrm{OS}} - \delta\lambda_{1\overline{\mathrm{MS}}}, \tag{B73}$$

$$m^2_{\overline{\mathrm{MS}}} = m^2 + \delta m^2_{\mathrm{OS}} - \delta m^2_{\overline{\mathrm{MS}}}, \tag{B74}$$

$$h_{x\overline{\mathrm{MS}}} = h_x + \delta h_{x\mathrm{OS}} - \delta h_{x\overline{\mathrm{MS}}}, \tag{B75}$$

$$h_{y\overline{\mathrm{MS}}} = h_y + \delta h_{y\mathrm{OS}} - \delta h_{y\overline{\mathrm{MS}}}, \tag{B76}$$

$$g^2_{\overline{\mathrm{MS}}} = g^2 + \delta g^2_{\mathrm{OS}} - \delta g^2_{\overline{\mathrm{MS}}}, \tag{B77}$$

$$\bar{\sigma}_x{}^2_{\overline{\mathrm{MS}}} = \bar{\sigma}_x^2 + \delta\bar{\sigma}_x{}^2_{\mathrm{OS}} - \delta\bar{\sigma}_x{}^2_{\overline{\mathrm{MS}}}, \tag{B78}$$

$$\bar{\sigma}_y{}^2_{\overline{\mathrm{MS}}} = \bar{\sigma}_y^2 + \delta\bar{\sigma}_y{}^2_{\mathrm{OS}} - \delta\bar{\sigma}_y{}^2_{\overline{\mathrm{MS}}}. \tag{B79}$$

The vacuum effective potential minimum lies at $\bar{\sigma}_x = f_\pi$ and $\bar{\sigma}_y = \frac{(2f_K - f_\pi)}{\sqrt{2}}$. Using the above set of equations together with Eqs. (B49), (B51), (B56), (B59), (B62), (B65), and (B67)–(B70), one writes the scale Λ dependent running parameters in the $\overline{\mathrm{MS}}$ scheme as the following:

$$\lambda_{2\overline{\mathrm{MS}}}(\Lambda) = \lambda_2 + \lambda_{2\mathrm{FIN}} + \lambda_{2\mathrm{SCF}}, \tag{B80}$$

$$c_{\overline{\mathrm{MS}}}(\Lambda) = c + c_{\mathrm{FINTOT}} + c_{\mathrm{SCF}}, \tag{B81}$$

$$\lambda_{1\overline{\mathrm{MS}}}(\Lambda) = \lambda_1 + \lambda_{1\mathrm{FIN}} + \lambda_{1\mathrm{SCF}}, \tag{B82}$$

$$m^2_{\overline{\mathrm{MS}}}(\Lambda) = m^2 + m^2_{\mathrm{FIN}}, \tag{B83}$$

$$h_{x\overline{\mathrm{MS}}}(\Lambda) = h_x + h_{x\mathrm{FIN}}, \tag{B84}$$

$$h_{y\overline{\mathrm{MS}}}(\Lambda) = h_y + h_{y\mathrm{FIN}}, \tag{B85}$$

$$g^2_{\overline{\mathrm{MS}}}(\Lambda) = g^2 + \frac{N_c g^4}{(4\pi)^2}\mathrm{SCF}, \tag{B86}$$

$$\bar{\sigma}_{x\,\overline{\mathrm{MS}}}^{\,2}(\Lambda) = f_\pi^2 - \frac{4N_c m_u^2}{(4\pi)^2}\mathrm{SCF}, \tag{B87}$$

$$\bar{\sigma}_{y\,\overline{\mathrm{MS}}}^{\,2}(\Lambda) = \left(\frac{2f_K - f_\pi}{\sqrt{2}}\right)^2 - \frac{2N_c m_s^2}{(4\pi)^2}\mathrm{SCF}. \tag{B88}$$

In Eqs. (B80)–(B86), the parameters λ_2, c, λ_1, m^2, h_x, h_y, and g^2, have the tree-level values of the QM model when $\bar{\sigma}_x = f_\pi$ and $\bar{\sigma}_y = \frac{(2f_K - f_\pi)}{\sqrt{2}}$ in the vacuum.

The parameters $\lambda_{2\overline{\mathrm{MS}}}$, $c_{\overline{\mathrm{MS}}}$, $\lambda_{1\overline{\mathrm{MS}}}$, $m^2_{\overline{\mathrm{MS}}}$, $h_{x\overline{\mathrm{MS}}}$, $h_{y\overline{\mathrm{MS}}}$, and $g^2_{\overline{\mathrm{MS}}}$ in the large N_c limit are running with the scale Λ and satisfy the following set of simultaneous renormalization group equations:

$$\frac{d\lambda_{2\overline{\mathrm{MS}}}(\Lambda)}{d\ln(\Lambda)} = \frac{2N_c}{(4\pi)^2}[2\lambda_{2\overline{\mathrm{MS}}} g^2_{\overline{\mathrm{MS}}} - g^4_{\overline{\mathrm{MS}}}], \tag{B89}$$

$$\frac{dc_{\overline{\mathrm{MS}}}(\Lambda)}{d\ln(\Lambda)} = \frac{3N_c}{(4\pi)^2} g^2_{\overline{\mathrm{MS}}} c_{\overline{\mathrm{MS}}}, \tag{B90}$$

$$\frac{d\lambda_{1\overline{\mathrm{MS}}}(\Lambda)}{d\ln(\Lambda)} = \frac{4N_c}{(4\pi)^2} g^2_{\overline{\mathrm{MS}}} \lambda_{1\overline{\mathrm{MS}}}, \tag{B91}$$

$$\frac{dm^2_{\overline{\mathrm{MS}}}(\Lambda)}{d\ln(\Lambda)} = \frac{2N_c}{(4\pi)^2} g^2_{\overline{\mathrm{MS}}} m^2_{\overline{\mathrm{MS}}}, \tag{B92}$$

$$\frac{dh_{x\overline{\mathrm{MS}}}(\Lambda)}{d\ln(\Lambda)} = \frac{N_c}{(4\pi)^2} g^2_{\overline{\mathrm{MS}}} h_{x\overline{\mathrm{MS}}}, \tag{B93}$$

$$\frac{dh_{y\overline{\mathrm{MS}}}(\Lambda)}{d\ln(\Lambda)} = \frac{N_c}{(4\pi)^2} g^2_{\overline{\mathrm{MS}}} h_{y\overline{\mathrm{MS}}}, \tag{B94}$$

$$\frac{dg^2_{\overline{\mathrm{MS}}}}{d\ln(\Lambda)} = \frac{2N_c}{(4\pi)^2} g^4_{\overline{\mathrm{MS}}}, \tag{B95}$$

$$\frac{d\bar{\sigma}_{x\,\overline{\mathrm{MS}}}^{\,2}}{d\ln(\Lambda)} = -\frac{2N_c}{(4\pi)^2} g^2_{\overline{\mathrm{MS}}} \bar{\sigma}_{x\,\overline{\mathrm{MS}}}^{\,2}, \tag{B96}$$

$$\frac{d\bar{\sigma}_{y\,\overline{\mathrm{MS}}}^{\,2}}{d\ln(\Lambda)} = -\frac{2N_c}{(4\pi)^2} g^2_{\overline{\mathrm{MS}}} \bar{\sigma}_{y\,\overline{\mathrm{MS}}}^{\,2}. \tag{B97}$$

The differential Eqs. (B89)–(B97) have the following solutions:

$$\lambda_{2\overline{\mathrm{MS}}}(\Lambda) = \frac{\lambda_{20} - \frac{N_c g_0^4}{(4\pi)^2}\ln\left(\frac{\Lambda^2}{\Lambda_0^2}\right)}{\left(1 - \frac{N_c g_0^2}{(4\pi)^2}\ln\left(\frac{\Lambda^2}{\Lambda_0^2}\right)\right)^2}, \tag{B98}$$

$$c_{\overline{\mathrm{MS}}}(\Lambda) = \frac{c_0}{\sqrt{\left[1 - \frac{N_c g_0^2}{(4\pi)^2}\ln\left(\frac{\Lambda^2}{\Lambda_0^2}\right)\right]^3}}, \tag{B99}$$

$$\lambda_{1\overline{\mathrm{MS}}}(\Lambda) = \frac{\lambda_{10}}{\left(1 - \frac{N_c g_0^2}{(4\pi)^2}\ln\left(\frac{\Lambda^2}{\Lambda_0^2}\right)\right)^2}, \tag{B100}$$

$$m^2_{\overline{\mathrm{MS}}}(\Lambda) = \frac{m_0^2}{1 - \frac{N_c g_0^2}{(4\pi)^2}\ln\left(\frac{\Lambda^2}{\Lambda_0^2}\right)}, \tag{B101}$$

$$h_{x\overline{\mathrm{MS}}}(\Lambda) = \frac{h_{x0}}{\sqrt{1 - \frac{N_c g_0^2}{(4\pi)^2}\ln\left(\frac{\Lambda^2}{\Lambda_0^2}\right)}}, \tag{B102}$$

$$h_{y\overline{\mathrm{MS}}}(\Lambda) = \frac{h_{y0}}{\sqrt{1 - \frac{N_c g_0^2}{(4\pi)^2}\ln\left(\frac{\Lambda^2}{\Lambda_0^2}\right)}}, \tag{B103}$$

$$g^2_{\overline{\mathrm{MS}}}(\Lambda) = \frac{g_0^2}{1 - \frac{N_c g_0^2}{(4\pi)^2}\ln\left(\frac{\Lambda^2}{\Lambda_0^2}\right)}, \tag{B104}$$

$$\bar{\sigma}^2_{x\,\overline{\mathrm{MS}}} = f_\pi^2\left[1 - \frac{N_c g_0^2}{(4\pi)^2}\ln\left(\frac{\Lambda^2}{\Lambda_0^2}\right)\right], \tag{B105}$$

$$\bar{\sigma}_{y\,\overline{\mathrm{MS}}}^{\,2} = \frac{(2f_K - f_\pi)^2}{2}\left[1 - \frac{N_c g_0^2}{(4\pi)^2}\ln\left(\frac{\Lambda^2}{\Lambda_0^2}\right)\right]. \tag{B106}$$

Here, λ_{10}, λ_{20}, g_0^2, m_0^2, c_0, h_{x0}, and h_{y0} are the values of the running parameters at scale Λ_0. The Λ_0 can be chosen such as to satisfy the following relation:

$$\ln\left(\frac{\Lambda_0^2}{m_u^2}\right) + \mathcal{C}(m_\pi^2) + m_\pi^2 \mathcal{C}'(m_\pi^2) = 0. \tag{B107}$$

The parameters of Eqs. (B80)–(B88) are obtained at the scale $\Lambda = \Lambda_0$.

1. Derivation of the effective potential

The values of the parameters in Eqs. (B98)–(B104) can be used to find the expression of the vacuum effective potential in the $\overline{\rm MS}$ scheme as the following:

$$\Omega_{\rm vac} = U(\bar{\sigma}_{x\overline{\rm MS}}, \bar{\sigma}_{y\overline{\rm MS}}) + \Omega^{q,{\rm vac}}_{\overline{\rm MS}} + \delta U(\bar{\sigma}_{x\overline{\rm MS}}, \bar{\sigma}_{y\overline{\rm MS}}), \tag{B108}$$

where

$$\begin{aligned} U(\bar{\sigma}_{x\overline{\rm MS}}, \bar{\sigma}_{y\overline{\rm MS}}) &= \frac{m^2_{\overline{\rm MS}}}{2}(\bar{\sigma}_{x\overline{\rm MS}}^2 + \bar{\sigma}_{y\overline{\rm MS}}^2) - h_{x\overline{\rm MS}}\bar{\sigma}_{x\overline{\rm MS}} - h_{y\overline{\rm MS}}\bar{\sigma}_{y\overline{\rm MS}} - \frac{c_{\overline{\rm MS}}}{2\sqrt{2}}\bar{\sigma}_{x\overline{\rm MS}}^2\bar{\sigma}_{y\overline{\rm MS}} + \frac{\lambda_{1\overline{\rm MS}}}{2}\bar{\sigma}_{x\overline{\rm MS}}^2\bar{\sigma}_{y\overline{\rm MS}}^2 \\ &+ \frac{(2\lambda_{1\overline{\rm MS}} + \lambda_{2\overline{\rm MS}})}{8}\bar{\sigma}_{x\overline{\rm MS}}^4 + \frac{2(\lambda_{1\overline{\rm MS}} + \lambda_{2\overline{\rm MS}})}{8}\bar{\sigma}_{y\overline{\rm MS}}^4, \end{aligned} \tag{B109}$$

$$\begin{aligned} \delta U(\bar{\sigma}_{x\overline{\rm MS}}, \bar{\sigma}_{y\overline{\rm MS}}) &= \frac{\delta m^2_{\overline{\rm MS}}}{2}(\bar{\sigma}_{x\overline{\rm MS}}^2 + \bar{\sigma}_{y\overline{\rm MS}}^2) + \frac{m^2_{\overline{\rm MS}}}{2}(\delta\bar{\sigma}_{x\overline{\rm MS}}^2 + \delta\bar{\sigma}_{y\overline{\rm MS}}^2) - \delta h_{x\overline{\rm MS}}\bar{\sigma}_{x\overline{\rm MS}} - h_{x\overline{\rm MS}}\delta\bar{\sigma}_{x\overline{\rm MS}} - \delta h_{y\overline{\rm MS}}\bar{\sigma}_{y\overline{\rm MS}} - h_{y\overline{\rm MS}}\delta\bar{\sigma}_{y\overline{\rm MS}} \\ &- \frac{\delta c_{\overline{\rm MS}}}{2\sqrt{2}}\bar{\sigma}_{x\overline{\rm MS}}^2\bar{\sigma}_{y\overline{\rm MS}} - \frac{c_{\overline{\rm MS}}}{2\sqrt{2}}(\delta\bar{\sigma}_{x\overline{\rm MS}}^2\bar{\sigma}_{y\overline{\rm MS}} + \bar{\sigma}_{x\overline{\rm MS}}^2\delta\bar{\sigma}_{y\overline{\rm MS}}) + \frac{\delta\lambda_{1\overline{\rm MS}}}{2}\bar{\sigma}_{x\overline{\rm MS}}^2\bar{\sigma}_{y\overline{\rm MS}}^2 + \frac{\lambda_{1\overline{\rm MS}}}{2}(\delta\bar{\sigma}_{x\overline{\rm MS}}^2\bar{\sigma}_{y\overline{\rm MS}}^2 + \bar{\sigma}_{x\overline{\rm MS}}^2\delta\bar{\sigma}_{y\overline{\rm MS}}^2) \\ &+ \left(\frac{2\delta\lambda_{1\overline{\rm MS}} + \delta\lambda_{2\overline{\rm MS}}}{8}\right)\bar{\sigma}_{x\overline{\rm MS}}^4 + \left(\frac{2\lambda_{1\overline{\rm MS}} + \lambda_{2\overline{\rm MS}}}{8}\right)\delta\bar{\sigma}_{x\overline{\rm MS}}^4 + \left(\frac{2\delta\lambda_{1\overline{\rm MS}} + 2\delta\lambda_{2\overline{\rm MS}}}{8}\right)\bar{\sigma}_{y\overline{\rm MS}}^4 \\ &+ \left(\frac{2\lambda_{1\overline{\rm MS}} + 2\lambda_{2\overline{\rm MS}}}{8}\right)\delta\bar{\sigma}_{y\overline{\rm MS}}^4. \end{aligned} \tag{B110}$$

Dropping the two loop terms $[\mathcal{O}(N_c^2)]$, we get

$$\delta U(\bar{\sigma}_{x\overline{\rm MS}}, \bar{\sigma}_{y\overline{\rm MS}}) = -\frac{N_c g^4_{\overline{\rm MS}}(\bar{\sigma}_{x\overline{\rm MS}}^4 + 2\bar{\sigma}_{y\overline{\rm MS}}^4)}{8(4\pi)^2}\frac{1}{\epsilon} = -\frac{N_c(2\Delta_x^4 + \Delta_y^4)}{(4\pi)^2}\frac{1}{\epsilon}. \tag{B111}$$

One writes the quark one-loop vacuum correction for the two nonstrange quark and the one strange quark flavor as

$$\begin{aligned} \Omega^{q,{\rm vac}}_{\overline{\rm MS}} &= \frac{N_c g^4_{\overline{\rm MS}}\bar{\sigma}_{x\overline{\rm MS}}^4}{8(4\pi)^2}\left[\frac{1}{\epsilon} + \frac{3}{2} + \ln\left(\frac{4\Lambda^2}{g^2_{\overline{\rm MS}}\bar{\sigma}_{x\overline{\rm MS}}^2}\right)\right] + \frac{N_c g^4_{\overline{\rm MS}} 2\bar{\sigma}_{y\overline{\rm MS}}^4}{8(4\pi)^2}\left[\frac{1}{\epsilon} + \frac{3}{2} + \ln\left(\frac{2\Lambda^2}{g^2_{\overline{\rm MS}}\bar{\sigma}_{y\overline{\rm MS}}^2}\right)\right] \\ &= \frac{2N_c\Delta_x^4}{(4\pi)^2}\left[\frac{1}{\epsilon} + \frac{3}{2} + \ln\left(\frac{\Lambda^2}{\Delta_x^2}\right)\right] + \frac{N_c\Delta_y^4}{(4\pi)^2}\left[\frac{1}{\epsilon} + \frac{3}{2} + \ln\left(\frac{\Lambda^2}{\Delta_y^2}\right)\right]. \end{aligned} \tag{B112}$$

The scale Λ independent parameters $\Delta_x = \frac{g_{\overline{\rm MS}}\bar{\sigma}_{x\overline{\rm MS}}}{2}$ and $\Delta_y = \frac{g_{\overline{\rm MS}}\bar{\sigma}_{y\overline{\rm MS}}}{\sqrt{2}}$ are defined by the use of Eqs. (B86)–(B88). Equation (B109) is written in terms of the scale independent Δ_x and Δ_y as

$$\begin{aligned} U(\Delta_x, \Delta_y) &= \frac{m^2_{\overline{\rm MS}}(\Lambda)}{g^2_{\overline{\rm MS}}(\Lambda)}(2\Delta_x^2 + \Delta_y^2) - 2\frac{h_{x\overline{\rm MS}}(\Lambda)}{g_{\overline{\rm MS}}(\Lambda)}\Delta_x - \sqrt{2}\frac{h_{y\overline{\rm MS}}(\Lambda)}{g_{\overline{\rm MS}}(\Lambda)}\Delta_y - 2\frac{c_{\overline{\rm MS}}(\Lambda)}{g^3_{\overline{\rm MS}}(\Lambda)}\Delta_x^2\Delta_y + 4\frac{\lambda_{1\overline{\rm MS}}(\Lambda)}{g^4_{\overline{\rm MS}}(\Lambda)}\Delta_x^2\Delta_y^2 \\ &+ 2\frac{(2\lambda_{1\overline{\rm MS}} + \lambda_{2\overline{\rm MS}})}{g^4_{\overline{\rm MS}}(\Lambda)}\Delta_x^4 + \frac{(\lambda_{1\overline{\rm MS}} + \lambda_{2\overline{\rm MS}})}{g^4_{\overline{\rm MS}}(\Lambda)}\Delta_y^4, \end{aligned} \tag{B113}$$

$$U(\Delta_x, \Delta_y) = \frac{m_0^2}{g_0^2}(2\Delta_x^2 + \Delta_y^2) - 2\frac{h_{x0}}{g_0}\Delta_x - \sqrt{2}\frac{h_{y0}}{g_0}\Delta_y - 2\frac{c_0}{g_0^3}\Delta_x^2\Delta_y + 4\frac{\lambda_{10}}{g_0^4}\Delta_x^2\Delta_y^2 + 2\frac{(2\lambda_{10} + \lambda_{20})}{g_0^4}\Delta_x^4 + \frac{(\lambda_{10} + \lambda_{20})}{g_0^4}\Delta_y^4, \tag{B114}$$

$$\Omega_{\rm vac}(\Delta_x,\Delta_y)=\frac{m_0^2}{g_0^2}(2\Delta_x^2+\Delta_y^2)-2\frac{h_{x0}}{g_0}\Delta_x-\sqrt{2}\frac{h_{y0}}{g_0}\Delta_y-2\frac{c_0}{g_0^3}\Delta_x^2\Delta_y+4\frac{\lambda_{10}}{g_0^4}\Delta_x^2\Delta_y^2+2\frac{(2\lambda_{10}+\lambda_{20})}{g_0^4}\Delta_x^4 + \frac{(\lambda_{10}+\lambda_{20})}{g_0^4}\Delta_y^4+\frac{2N_c\Delta_x^4}{(4\pi)^2}\left[\frac{3}{2}+\ln\left(\frac{\Lambda^2}{\Delta_x^2}\right)\right]+\frac{N_c\Delta_y^4}{(4\pi)^2}\left[\frac{3}{2}+\ln\left(\frac{\Lambda^2}{\Delta_y^2}\right)\right]. \tag{B115}$$

Expressing the mass parameter and the couplings in terms of the physical masses of mesons, the pion decay constant, the kaon decay constant, and Yukawa coupling, we write

$$\Omega_{\rm vac}(\Delta_x,\Delta_y)=\frac{(m^2+m_{\rm FIN}^2)}{2}\left\{f_\pi^2\left(\frac{\Delta_x^2}{m_u^2}\right)+\frac{(2f_K-f_\pi)^2}{2}\left(\frac{\Delta_y^2}{m_s^2}\right)\right\}-(h_x+h_{x\rm FIN})f_\pi\left(\frac{\Delta_x}{m_u}\right)-(h_y+h_{y\rm FIN})\frac{(2f_K-f_\pi)}{\sqrt{2}} \times\left(\frac{\Delta_y}{m_s}\right)-\frac{(c+c_{\rm FINTOT})}{4}f_\pi^2(2f_K-f_\pi)\left(\frac{\Delta_x^2}{m_u^2}\right)\left(\frac{\Delta_y}{m_s}\right)+\frac{(\lambda_1+\lambda_{1\rm FIN})}{4}f_\pi^2(2f_K-f_\pi)^2\left(\frac{\Delta_x^2}{m_u^2}\right)\left(\frac{\Delta_y^2}{m_s^2}\right) +\frac{\{2(\lambda_1+\lambda_{1\rm FIN})+(\lambda_2+\lambda_{2\rm FIN})\}}{8}f_\pi^4\left(\frac{\Delta_x^4}{m_u^4}\right)+\frac{\{(\lambda_1+\lambda_{1\rm FIN})+(\lambda_2+\lambda_{2\rm FIN})\}}{16}(2f_K-f_\pi)^4\left(\frac{\Delta_y^4}{m_s^4}\right) +\frac{2N_c\Delta_x^4}{(4\pi)^2}\left[\frac{3}{2}-\ln\left(\frac{\Delta_x^2}{m_u^2}\right)-\mathcal{C}(m_\pi^2)-m_\pi^2\mathcal{C}'(m_\pi^2)\right]+\frac{N_c\Delta_y^4}{(4\pi)^2}\left[\frac{3}{2}-\ln\left(\frac{\Delta_y^2}{m_u^2}\right)-\mathcal{C}(m_\pi^2)-m_\pi^2\mathcal{C}'(m_\pi^2)\right]. \tag{B116}$$

One notes that due to the dressing of the meson propagator in the on-shell scheme of the RQM model, the pion decay constant, the kaon decay constant, and Yukawa coupling get renormalized in the vacuum. But Eqs. (B86)–(B88) at the scale Λ_0 give us $g_{\overline{\rm MS}}=g_{\rm ren}=g$, $\bar{\sigma}_{x\overline{\rm MS}}=f_{\pi,\rm ren}=f_\pi$, and $\bar{\sigma}_{y\overline{\rm MS}}=\frac{2f_{K,\rm ren}-f_{\pi,\rm ren}}{\sqrt{2}}=\frac{2f_K-f_\pi}{\sqrt{2}}$. When the stationarity condition $\frac{\partial\Omega_{\rm vac}(\Delta_x,\Delta_y)}{\partial\Delta_x}=0$ is applied to Eq. (B116) in the nonstrange direction, one gets $h_{x0}=m_{\pi,c}^2\bar{\sigma}_{x\overline{\rm MS}}=m_\pi^2\{1-\frac{N_cg^2}{(4\pi)^2}m_\pi^2\mathcal{C}'(m_\pi^2)\}f_\pi$. Hence, the pion curvature mass $m_{\pi,c}^2=m_\pi^2\{1-\frac{N_cg^2}{(4\pi)^2}m_\pi^2\mathcal{C}'(m_\pi^2)\}$. The implementation of the stationarity condition $\frac{\partial\Omega_{\rm vac}(\Delta_x,\Delta_y)}{\partial\Delta_y}=0$ in the strange direction gives $h_{0y}=(\frac{\bar{\sigma}_{x\overline{\rm MS}}}{\sqrt{2}}+\bar{\sigma}_{y\overline{\rm MS}})m_{K,c}^2-\frac{\bar{\sigma}_{x\overline{\rm MS}}}{\sqrt{2}}m_{\pi,c}^2=\sqrt{2}f_Km_{K,c}^2-\frac{f_\pi}{\sqrt{2}}m_{\pi,c}^2$. One finds the expression of the kaon curvature mass $m_{K,c}^2$ as given below in Eq. (B117) by using the expression of $h_{y\overline{\rm MS}}(\Lambda_0)=h_{y0}$ in Eq. (B85). It is worth emphasizing that the pion curvature mass $m_{\pi,c}$ (as in Ref. [72]) and the kaon curvature mass are different from their pole masses m_π and m_K due to the consistent on-shell parameter fixing. The minimum of the effective potential remains fixed at $\bar{\sigma}_{x\overline{\rm MS}}=f_\pi$ and $\bar{\sigma}_{y\overline{\rm MS}}=\frac{(2f_K-f_\pi)}{\sqrt{2}}$,

$$m_{K,c}^2=m_K^2\left[1-\frac{N_cg^2}{(4\pi)^2}\left\{\mathcal{C}(m_\pi^2,m_u)+m_\pi^2\mathcal{C}'(m_\pi^2,m_u)-\left(1-\frac{(m_s-m_u)^2}{m_K^2}\right)\mathcal{C}(m_K^2,m_u,m_s) +\left(1-\frac{f_\pi}{f_K}\right)\frac{m_u^2-m_s^2+2m_s^2\ln(\frac{m_s}{m_u})}{m_K^2}\right\}\right]. \tag{B117}$$

[1] N. Cabibbo and G. Parisi, Phys. Lett. **59B**, 67 (1975).
[2] L. D. McLerran and B. Svetitsky, Phys. Rev. D **24**, 450 (1981); B. Svetitsky, Phys. Rep. **132**, 1 (1986).
[3] B. Muller, Rep. Prog. Phys. **58**, 611 (1995).
[4] H. Meyer-Ortmanns, Rev. Mod. Phys. **68**, 473 (1996).
[5] D. H. Rischke, Prog. Part. Nucl. Phys. **52**, 197 (2004).
[6] A. Ali Khan *et al.*, Phys. Rev. D **64**, 074510 (2001).
[7] S. Digal, E. Laermann, and H. Satz, Eur. Phys. J. C **18**, 583 (2001).
[8] F. Karsch, Lect. Notes Phys. **583**, 209 (2002).
[9] Z. Fodor, S. D. Katz, and K. K. Szabo, Phys. Lett. B **568**, 73 (2003).
[10] C. R. Allton, M. Doring, S. Ejiri, S. J. Hands, O. Kaczmarek, F. Karsch, E. Laermann, and K. Redlich, Phys. Rev. D **71**, 054508 (2005).
[11] F. Karsch, J. Phys. G **31**, S633 (2005).
[12] Y. Aoki, Z. Fodor, S. D. Katz, and K. K. Szabo, Phys. Lett. B **643**, 46 (2006).
[13] M. Cheng *et al.*, Phys. Rev. D **74**, 054507 (2006).
[14] M. Cheng *et al.*, Phys. Rev. D **77**, 014511 (2008).
[15] J. Langelage, S. Lottini, and O. Philipsen, J. High Energy Phys. 02 (2011) 057.
[16] M. G. Alford, A. Schmitt, and K. Rajagopal, Rev. Mod. Phys. **80**, 1455 (2008).
[17] K. Fukushima and T. Hatsuda, Rep. Prog. Phys. **74**, 014001 (2011).
[18] G. Fejos, Phys. Rev. D **92**, 036011 (2015).
[19] G. Fejos and A. Hosaka, Phys. Rev. D **94**, 036005 (2016).
[20] Fabian Rennecke and Bernd-Jochen Schaefer, Phys. Rev. D **96**, 016009 (2017).
[21] G. Fejos and A. Hosaka, Phys. Rev. D **98**, 036009 (2018).
[22] G. Fejos and A. Patkos, Phys. Rev. D **105**, 096007 (2022).
[23] G. 't Hooft, Phys. Rev. Lett. **37**, 8 (1976).
[24] J. T. Lenaghan, D. H. Rischke, and J. Schaffner-Bielich, Phys. Rev. D **62**, 085008 (2000). J. T. Lenaghan and D. H. Rischke, J. Phys. G **26**, 431 (2000).
[25] B. J. Schaefer and M. Wagner, Phys. Rev. D **79**, 014018 (2009).
[26] D. Roder, J. Ruppert, and D. H. Rischke, Phys. Rev. D **68**, 016003 (2003).
[27] K. Fukushima, K. Kamikado, and B. Klein, Phys. Rev. D **83**, 116005 (2011).
[28] M. Grahl and D. H. Rischke, Phys. Rev. D **88**, 056014 (2013).
[29] A. Jakovac, A. Patkos, Z. Szep, and P. Szepfalusy, Phys. Lett. B **582**, 179 (2004).
[30] T. Herpay, A. Patkós, Zs. Szép, and P. Szépfalusy, Phys. Rev. D **71**, 125017 (2005).
[31] T. Herpay and Zs. Szép, Phys. Rev. D **74**, 025008 (2006).
[32] P. Kovács and Zs. Szép, Phys. Rev. D **75**, 025015 (2007).
[33] P. Kovacs and Zs. Szep, Phys. Rev. D **75**, 025015 (2007).
[34] T. Kahara and K. Tuominen, Phys. Rev. D **78**, 034015 (2008); **80**, 114022 (2009); **82**, 114026 (2010).
[35] E. S. Bowman and J. I. Kapusta, Phys. Rev. C **79**, 015202 (2009); J. I. Kapusta and E. S. Bowman, Nucl. Phys. **A830**, 721C (2009).
[36] G. Fejos and A. Patkos, Phys. Rev. D **82**, 045011 (2010).
[37] A. Jakovac and Zs. Szep, Phys. Rev. D **82**, 125038 (2010).
[38] L. Ferroni, V. Koch, and M. B. Pinto, Phys. Rev. C **82**, 055205 (2010).
[39] G. Marko and Zs. Szep, Phys. Rev. D **82**, 065021 (2010).
[40] O. Scavenuius, A. Mocsy, I. N. Mishustin, and D. H. Rischke, Phys. Rev. C **64**, 045202 (2001).
[41] A. Mocsy, I. N. Mishustin, and P. J. Ellis, Phys. Rev. C **70**, 015204 (2004).
[42] B.-J. Schaefer and J. Wambach, Nucl. Phys. **A757**, 479 (2005).
[43] B.-J. Schaefer and J. Wambach, Phys. Rev. D **75**, 085015 (2007).
[44] R. D. Pisarski and F. Wilczek, Phys. Rev. D **29**, 338 (1984).
[45] A. Halasz, A. D. Jackson, R. E. Shrock, M. A. Stephanov, and J. J. M. Verbaarschot, Phys. Rev. D **58**, 096007 (1998).
[46] V. Skokov, B. Friman, E. Nakano, K. Redlich, and B.-J. Schaefer, Phys. Rev. D **82**, 034029 (2010).
[47] R. Gatto and M. Ruggieri, Phys. Rev. D **82**, 054027 (2010).
[48] *Strongly Interacting Matter in Magnetic Fields*, edited by D. Kharzeev, K. Landsteiner, A. Schmitt, and H.-U. Yee, Lecture Notes in Physics Vol. 871 (Springer, New York, 2013).
[49] A. J. Mizher, M. N. Chernodub, and E. S. Fraga, Phys. Rev. D **82**, 105016 (2010).
[50] M. Drew and W. Weise, Phys. Rev. C **91**, 035802 (2015); Prog. Part. Nucl. Phys. **93**, 69 (2017).
[51] L. Brandes, N. Kaiser, and W. Weise, Eur. Phys. J. A **57**, 243 (2021).
[52] Andreas Zacchi and Jürgen Schaffner-Bielich, Phys. Rev. D **97**, 074011 (2018).
[53] Andreas Zacchi and Jürgen Schaffner-Bielich, Phys. Rev. D **100**, 123024 (2019).
[54] L. F. Palhares and E. S. Fraga, Phys. Rev. D **78**, 025013 (2008).
[55] E. S. Fraga, L. F. Palhares, and M. B. Pinto, Phys. Rev. D **79**, 065026 (2009).
[56] L. F. Palhares and E. S. Fraga, Phys. Rev. D **82**, 125018 (2010).
[57] R. Khan and L. T. Kyllingstad, AIP Conf. Proc. **1343**, 504 (2011).
[58] U. S. Gupta and V. K. Tiwari, Phys. Rev. D **85**, 014010 (2012).
[59] B.-J. Schaefer and M. Wagner, Phys. Rev. D **85**, 034027 (2012).
[60] S. Chatterjee and K. A. Mohan, Phys. Rev. D **85**, 074018 (2012).
[61] V. K. Tiwari, Phys. Rev. D **86**, 094032 (2012).
[62] J. O. Andersen and A. Tranberg, J. High Energy Phys. 08 (2012) 002.
[63] S. Chatterjee and K. A. Mohan, Phys. Rev. D **86**, 114021 (2012).
[64] V. K. Tiwari, Phys. Rev. D **88**, 074017 (2013).
[65] T. K. Herbst, J. M. Pawlowski, and B.-J. Schaefer, Phys. Rev. D **88**, 014007 (2013).
[66] J. Weyrich, N. Strodthoff, and L. von Smekal, Phys. Rev. C **92**, 015214 (2015).
[67] P. Kovács, Zs Szép, and Gy Wolf, Phys. Rev. D **93**, 114014 (2016).
[68] S. K. Rai and V. K. Tiwari, Eur. Phys. J. Plus **135**, 844 (2020).

[69] K. Kajantie, M. Laine, K. Rummukainen, and M. E. Shaposhnikov, Nucl. Phys. **B458**, 90 (1996).
[70] P. Adhikari, J. O. Andersen, and P. Kneschke, Phys. Rev. D **95**, 036017 (2017).
[71] S. Carignano, M. Buballa, and B.-J. Schaefer, Phys. Rev. D **90**, 014033 (2014).
[72] S. Carignano, M. Buballa, and W. Elkamhawy, Phys. Rev. D **94**, 034023 (2016).
[73] J. O. Andersen, W. R. Naylor, and A. Tranberg, Rev. Mod. Phys. **88**, 025001 (2016).
[74] R. Kobes, G. Kunstatter, and A. Rebhan, Phys. Rev. Lett. **64**, 2992 (1990); Nucl. Phys. **B355**, 1 (1991).
[75] A. K. Rebhan, Phys. Rev. D **48**, R3967 (1993).
[76] P. Adhikari, J. O. Andersen, and P. Kneschke, Phys. Rev. D **96**, 016013 (2017).
[77] P. Adhikari, J. O. Andersen, and P. Kneschke, Phys. Rev. D **98**, 074016 (2018).
[78] A. Folkestad and J. O. Andersen, Phys. Rev. D **99**, 054006 (2019).
[79] S. K. Rai and V. K. Tiwari, Phys. Rev. D **105**, 094010 (2022).
[80] V. K. Tiwari, Phys. Rev. D **108**, 074002 (2023).
[81] A. M. Polyakov, Phys. Lett. **72B**, 477 (1978).
[82] B. Svetitsky and L. G. Yaffe, Nucl. Phys. **B210**, 423 (1982).
[83] T. Banks and A. Ukawa, Nucl. Phys. **B225**, 145 (1983).
[84] R. D. Pisarski, Phys. Rev. D **62**, 111501(R) (2000).
[85] K. Fukushima, Phys. Lett. B **591**, 277 (2004).
[86] B. Layek, A. P. Mishra, A. M. Srivastava, and V. K. Tiwari, Phys. Rev. D **73**, 103514 (2006).
[87] C. Ratti, M. A. Thaler, and W. Weise, Phys. Rev. D **73**, 014019 (2006).
[88] S. Roessner, C. Ratti, and W. Weise, Phys. Rev. D **75**, 034007 (2007).
[89] K. Fukushima, Phys. Rev. D **78**, 114019 (2008).
[90] B. J. Schaefer, J. M. Pawlowski, and J. Wambach, Phys. Rev. D **76**, 074023 (2007).
[91] B. J. Schaefer, M. Wagner, and J. Wambach, Proc. Sci. CPOD2009 (**2009**) 017.
[92] B. J. Schaefer, M. Wagner, and J. Wambach, Phys. Rev. D **81**, 074013 (2010).
[93] H. Mao, J. Jin, and M. Huang, J. Phys. G **37**, 035001.
[94] U. S. Gupta and V. K. Tiwari, Phys. Rev. D **81**, 054019 (2010).
[95] S. K. Rai and V. K. Tiwari, Phys. Rev. D **108**, 074014 (2023).
[96] L. M. Haas, R. Stiele, J. Braun, J. M. Pawlowski, and J. Schaffner-Bielich, Phys. Rev. D **87**, 076004 (2013).
[97] P. M. Lo, B. Friman, O. Kaczmarek, K. Redlich, and C. Sasaki, Phys. Rev. D **88**, 074502 (2013).
[98] T. K. Herbst, M. Mitter, J. M. Pawlowski, and B.-J. Schaefer, and R. Stiele, Phys. Lett. B **731**, 248 (2014).
[99] R. Stiele and J. Schaffner-Bielich, Phys. Rev. D **93**, 094014 (2016).
[100] T. K. Herbst, J. M. Pawlowski, and B.-J. Schaefer, Phys. Lett. B **696**, 58 (2011).
[101] J. I. Kapusta and C. Gale, *Finite Temperature Field Theory Principles and Applications* (Cambridge University Press, Cambridge, England, 2006).
[102] S. Borsányi, Z. Fodor, C. Hoelbling, S. D. Katz, S. Krieg, C. Ratti, and K. K. Szabó, J. High Energy Phys. 09 (2010) 073.
[103] S. Borsanyi, G. Endrodi, Z. Fodor, A. Jakovac, S. D. Katz, S. Krieg, C. Ratti, and K. K. Szabo, J. High Energy Phys. 11 (2010) 077; S. Borsanyi, Z. Fodor, C. Hoelbling, S. D. Katz, S. Krieg, and K. K. Szabo, Phys. Lett. B **730**, 99 (2014).
[104] A. Bazavov *et al.*, Phys. Rev. D **90**, 094503 (2014).